Hydrogels for Local and Sustained Delivery of Bacteriophages to Treat Wound Infections

Yung-Hao Lin[1*], Tejas Dharmaraj[2*], Qingquan Chen[2*], Arne Echterhof[2,3], Robert Manasherob[4], Lucy Jia Zheng[5], Cas de Leeuw[6], Nana Ansuah Peterson[2], Whitney Stannard[2], Zhiwei Li[2], Maryam Hajfathalian[2,7], Aviv Hargil[2], Hunter A. Martinez[2], Tony Hong Wei Chang[2], Francis G. Blankenberg[8], Derek Amanatullah[4], Ovijit Chaudhuri[9]† and Paul L. Bollyky[2]†

[1]Department of Chemical Engineering, Stanford University, Stanford, CA, USA
[2]Division of Infectious Diseases and Geographic Medicine, Department of Medicine, Stanford University, Stanford, CA, USA
[3]Institute of Medical Microbiology, University Hospital of Muenster, Muenster, Germany
[4]Department of Orthopaedic Surgery, Stanford Hospital and Clinics, Redwood City, CA, USA
[5]Department of Material Science and Engineering, Stanford University, Stanford, CA, USA
[6]Institute for Molecules and Materials, Radboud University, Nijmegen, Netherlands
[7]Department of Biomedical Engineering, New Jersey Institute of Technology, University Heights, Newark, NJ
[8]Division of Pediatric Radiology and Nuclear Medicine, Department of Radiology, Lucile Packard Children's Hospital, Stanford, CA, USA
[9]Department of Mechanical Engineering, Stanford University, Stanford, CA, USA

[*] Authors contributed equally

† Address correspondence to pbollyky@stanford.edu and chaudhuri@stanford.edu

Abstract

Bacteriophages (phages) are viruses that specifically target and kill bacteria, serving as a promising therapeutic to combat multidrug-resistant (MDR) pathogens such as *Pseudomonas aeruginosa* (*Pa*). However, delivering adequate concentrations of active phages directly to the infection site over sufficient times to eradicate infections remains an outstanding challenge to phage therapy (PT). Here we present "HydroPhage", a biocompatible hydrogel system for the sustained release of high-titre phages to effectively treat infections caused by MDR pathogens. We develop injectable hydrogels comprised of hyaluronic acid (HA) and polyethylene glycol (PEG) crosslinked through static covalent thioether bonds and hemithioacetal-based dynamic covalent crosslinks (DCC), which encapsulate phages at concentration up to 10^{11} PFU per mL gel, and achieve sustained release over a week with more than 60% total phage recovery. In a preclinical mouse model of extended wound infection, we demonstrate enhanced bacterial clearance compared to intravenous treatment. Thus, using hydrogels for local and sustained delivery of phage may represent an effective approach to eradicating MDR infections broadly.

Introduction

Patients with chronic wounds are prone to infections [1], which typically require weekly treatments, including wound debridement, topical antimicrobials, and dressing changes, as part of the standard of care [2–6]. However, this current treatment regimen is often insufficient to eradicate infections, resulting in over 160,000 diabetic limb amputations are performed annually in the US [7].

Pseudomonas aeruginosa (Pa) is the most prevalent Gram-negative bacterium associated with wound infections, implicated in 25-50% of all chronic wounds [8–11]. Managing *Pa* infections presents a significant challenge due to its chromosomally encoded resistance mechanisms [12], leading to resistance against numerous antibiotics, including those considered as last-resort options [13–16]. Multidrug-resistant (MDR) *Pa* is recognized as a serious threat by the Centers for Disease Control and Prevention (CDC) and the World Health Organization (WHO)[17,18], but there are few antipseudomonal antibiotics in the clinical pipeline. Hence, there is an urgent need to identify alternative therapies against *Pa* wound infections.

Bacteriophages (phages) are viruses that specifically infect and kill bacteria [19]. They were first used to treat infections over 100 years ago [20], but the advent of antibiotics relegated phage therapy (PT) to the sidelines in most of the world [21]. With the rise of MDR pathogens, PT has regained interest among researchers and medical centers [21,22]. Phages offer several advantages as a treatment option against MDR *Pa* infections, including their high specificity toward target bacteria without perturbing the host microbiome [23], their potential to disrupt biofilms [24], and their general safety and tolerability [25–28]. As a result, there is substantial interest in using PT to treat wound infections [29–31] and in phage pharmacology [32,33].

However, how to best deliver phages to treat wound infections is unclear. In preclinical models, tissue concentrations of phages following systemic administration, including via oral, intraperitoneal, and intravenous (IV) delivery, are often low, with most phages cleared in the liver and spleen [34,35]. Phages can replicate at the site of infection ("active killing") [36,37], but it is unclear whether this is sufficient for bacterial elimination [38]. Patients with chronic wound infections have been administered phages of variable concentration and frequency [39,40]. High concentrations of phages have been applied directly to the wound bed with success in preclinical models [41–45]. However, the optimal concentrations and dosing frequency of PT remain uncertain.

In humans, locally administered phage treatments for chronic wounds have mainly been delivered via gauze or cellulose wound dressings soaked with phages [46,47]. However, these approaches have had variable success [40,43,46,48]. Better alternatives for local phage delivery are needed. Ideally, PT would integrate seamlessly into patients' chronic wound care regimens, in the form of an advanced dressing that can adhere to the skin and deliver effective local concentrations of therapeutics over a timeframe of a week, which aligns with the typical duration for outpatient wound care visits and debridement events [49].

Hydrogels are attractive as wound dressings and platforms for controlled topical phage delivery [45,50,51]. However, developing suitable wound dressings tailored for topical phage delivery, supported by proven preclinical models, has lagged [52,53]. Simply embedding phages in static, ionically crosslinked hydrogels will release most phages within 24 hours [54–56]. Fibrin glues, while allowing release over longer periods, offer no control over release kinetics and require shaking at high speed [57]. Covalently crosslinked hydrogels with protease-degradable polymer backbones provide release over longer timescales; however, release kinetics are dependent upon enzyme concentrations *in vivo*, which are uncontrollable [58]. Despite some case reports suggesting that

sustained release of phages using dressings or bandages soaked with phages is important for the clearance of infections in chronic wounds [30,31,59], the characterization of phage release kinetics has not been reported in these contexts. Hence, rational design of the hydrogel and the systematic evaluation of phage release kinetics and treatment efficacy are needed to advance phage delivery for topical treatments.

To address these deficiencies, we have developed an innovative hyaluronic acid (HA) and polyethylene glycol (PEG)-based hydrogel system for sustained and local delivery of phages. We call this combination of a hydrogel with phage that delivers phages in a sustained manner "HydroPhage" (HP). Here, we have used this delivery vehicle to assess phage release kinetics and antimicrobial capability. We find that HP can encapsulate phages at concentrations up to 10^{11} PFU/mL and release phages at concentrations around 10^{9} to 5×10^{10} PFU/mL daily over a week, with more than 60% total phage released. HP significantly reduces bacterial loads in planktonic and biofilm cultures of bacteria *in vitro*. Importantly, HP improved bacterial clearance in a novel, single treatment murine wound infection model.

Results

Dual-crosslinked HA and PEG based hydrogels are injectable

We developed a soft, injectable HA- and PEG-based hydrogel, specifically engineered to be compatible with extremely fine-gauge needles for precise application (**Fig. 1a**). This hydrogel is synthesized through a dual-crosslinking mechanism involving both covalent and dynamic covalent bonds. The covalent thioether bonds are formed between hyperbranched PEG multi-acrylate (HBPEG) and thiolated-hyaluronic acid (HA-SH), while dynamic covalent hemithioacetal linkages are created using 4-arm PEG-aldehyde or PEG-benzaldehyde crosslinkers (4ALD and 4BLD) that react with the thiols on HA-SH (**Fig. 1b**). These reactions occur spontaneously under physiological conditions, eliminating the need for harsh solvents or catalysts. Lytic phages, such as the antipseudomonal phage PAML-31-1 (**Fig. 1a**), can be mixed in with the polymer precursors prior to gelation.

We find that hydrogels with a combination of static covalent crosslinking (CC) and dynamic covalent crosslinking (DCC) presented higher and more rapid increase in stiffness, compared to hydrogels with CC or DCC alone (**Fig. 1c**). In addition, the fast kinetics of the DCC enables immediate enhancement of viscosity and adhesiveness without compromising injectability (**Supplementary Fig. 1a-b**). These features ensure easy application and secure adherence of the hydrogels to the irregular contours of infected wound surfaces.

Overall, the unique combination of viscosity, adhesivity, and injectability resulting from both CC and DCC makes this HA-PEG hydrogel particularly suitable for application to wound beds, offering ease of use and effective delivery of therapeutic agents.

HA-PEG hydrogels enable sustained release of high-titre phages

We then examined the release kinetics of phages from the HA-PEG hydrogels using phage PAML-31-1 initially. Hydrogels were formed within transwell inserts and then immersed in a minimal amount of buffer. The buffer was extracted after 1 day from the basolateral and apical chambers and combined, with the phage titre then measured using standard lytic plaque assays. Finally, the transwell was transferred to a new well containing fresh buffer (**Fig. 1d**).

We first sought to optimize our hydrogel formulation for sustained release over periods of up to a week, a typical time between clinic visits for wound debridement for patients with chronic wounds. A previous study showed that hydrogels formed via thiol-Michael addition require polymer degradation mechanisms, like protease-cleavable crosslinkers, to facilitate phage release [58]. We hypothesized that by utilizing a lower thioether crosslinking density, we could enhance phage release due to a looser polymer mesh and eliminate the need for additional polymer degradation mechanisms. Indeed, hydrogels with lower HBPEG concentrations led to higher phage recovery, suggesting denser covalent thioether crosslinks trapped phages and limited phage release (**Fig. 1e** and **Supplementary Fig. 2a, b**). Further investigation into hydrogels with low thioether crosslinking (1 mg/mL HBPEG) revealed that higher concentrations of 4ALD and 4BLD crosslinkers led to increased phage recovery (**Fig. 1f**). At high concentrations of 4ALD and 4BLD, a lower percentage of benzaldehyde (%BLD) crosslinkers corresponded to higher percent phage recovery and more sustained release from day 4 to 7. One explanation of this result is that the more stable polymer-polymer and polymer-phage bindings with benzaldehyde versus aldehyde limits phage release. In light of these data, the optimal HA-PEG hydrogel formulation for sustained

phage release was determined as: 5 mg/mL HA-SH, 1 mg/mL HBPEG, and 75 mg/mL of 4-arm PEGs with 10% 4BLD and 90% 4ALD. This hydrogel formulation was used for HydroPhage (HP) in the rest of the study.

Next, we investigated how phage titre affected the release kinetics. Surprisingly, higher encapsulated phage titres led to increased percent phage recovery; encapsulating 10^{11} PFU/mL in HP resulted in 62% phage recovery, compared to 28% recovery for 10^{10} PFU/mL and 21% recovery for 10^{9} PFU/mL (**Fig. 1g**). Higher titres may saturate the binding of aldehyde and benzaldehyde groups by phage capsids, allowing a larger portion of unbound phages to diffuse more freely.

Then, we examined how different phages behave in this system using three distinct *Pa*-targeting phages—Luz24, PAML-31-1, and LPS-5. All three phages exhibited comparable release kinetics (**Fig. 1h**). This emphasizes the potential of the HA-PEG hydrogel to deliver a broad spectrum of phages, or a cocktail of phages, tailored to specific infections. In contrast to an ionically crosslinked alginate (AG-Ca^{2+}) hydrogel, which exhibited burst release of nearly all encapsulated phages within the first 24 hours, the HA-PEG hydrogel exhibited sustained high-titre phage release (~10^{9} PFU/mL or higher) for up to 7 days (**Fig. 1i**).

Finally, we examined the mechanisms mediating phage release from HP. Amines on proteins on the phage surface could theoretically bind to aldehyde/benzaldehyde through dynamic covalent imine bonds, which could, in principle, delay phage release from HP, leading to sustained release [60–62]. Benzaldehyde groups are expected to form bonds with higher affinity than aldehyde groups [63,64]. However, varying the ratio of aldehyde to benzaldehyde did not have a strong effect on release, indicating DCC did not play a governing role in controlling phage release. In contrast, there was a close correspondence between the released phage percentage and the extent of polymer mass loss (**Fig. 1j**). Thus, hydrolytic erosion appears to be the primary driver of sustained phage release from HP. Overall, our dual-crosslinked HA-PEG hydrogel offers a novel and effective approach for the sustained delivery of high-titre phages to treat wound infections.

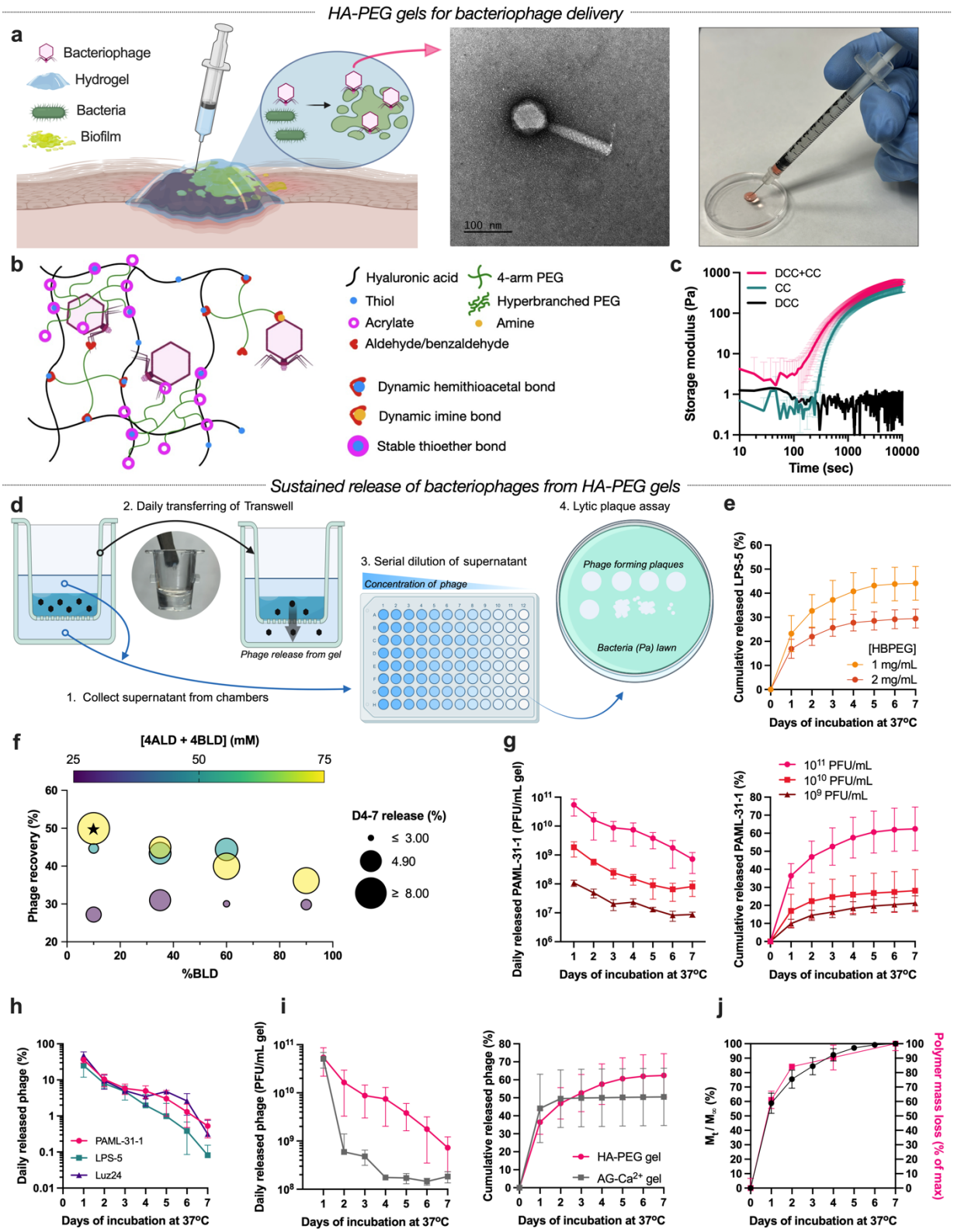

Fig. 1. HA-PEG hydrogel with dynamic covalent and static covalent crosslinks for sustained and topical delivery of high-dose bacteriophage. a, Schematic of phage release

from injectable hydrogel to combat bacteria and biofilm (left); PAML-31-1 phage visualized using transmission electron microscopy (TEM) (center). Scale bar = 100 nm; image of hyaluronic acid (HA)- and polyethylene glycol (PEG)-based hydrogel (HA-PEG) injected through a 28G needle (right). **b**, Schematic of HA-PEG hydrogel crosslinking chemistries. Covalent thioether crosslinks are formed between thiolated-HA (HA-SH) and hyperbranched PEG multi-acrylate (HBPEG). Dynamic covalent hemithioacetal crosslinks are formed between HA-SH with either 4-arm PEG-aldehyde (4ALD) or benzaldehyde (4BLD). Amines presented on the surface of phages could theoretically bind to aldehyde/benzaldehyde through dynamic covalent imine bonds. **c**, The storage modulus of hydrogels with both dynamic covalent crosslinking and covalent crosslinking (DCC+CC, magenta), covalent crosslinking alone (CC, green), and dynamic covalent crosslinking alone (DCC, black). Hydrogel formulations: 7 mg/mL HA-SH, 4 mg/mL HBPEG, and 75 mg/mL of 4-arm PEGs with 10% 4BLD and 90% 4ALD for DCC+CC gel; n = 4; 7 mg/mL HA-SH and 4 mg/mL HBPEG for CC gel; n = 3; 7 mg/mL HA-SH and 75 mg/mL of 4-arm PEGs with 10% 4BLD and 90% 4ALD for DCC gel; n = 1. **d**, Schematic of the transwell-release assay to quantify phage release from HA-PEG hydrogel daily. **e**, HBPEG of 1 mg/mL led to a higher percentage of phage recovery compared to 2 mg/m; n = 3 for each formulation. **f**, The HA-PEG hydrogel contained 5 mg/mL of HA-SH and 1 mg/mL of HBPEG, and the 4-arm PEGs concentration and %BLD were varied to explore the optimal hydrogel formulation with the highest percentage of recovery and sustained release. Sustained release was defined as the cumulative phage release from day 4 to 7, indicated by the size of the dots; n = 1 for each formulation. The star sign indicates the chosen hydrogel formulation for the rest of the study. **g**. Quantification of daily and cumulative release of PAML-31-1 phage out of HA-PEG hydrogel with different encapsulation titres: 10^{11}, 10^{10}, and 10^{9} PFU/mL; n = 8, 3, and 3, respectively. **h**, Quantification of daily release of different phages—PAML-31-1, LPS-5, and Luz24—from HA-PEG hydrogel with encapsulation titre of 10^{11} PFU/mL; n = 8, 4, and 2, respectively. **i**, Comparison of the daily and cumulative release of phage from HA-PEG hydrogel versus an ionically crosslinked alginate hydrogel (AG-Ca^{2+}) with encapsulation titre of 10^{11} PFU/mL; n = 8 and 4, respectively. **j**, Close correspondence between the percentage of maximum phage release, defined as the ratio of cumulative phage release at given time point (M_t) to the endpoint maximum cumulative release (M_∞), and the mass loss of HA-PEG hydrogel, defined as the percentage of mass loss to the maximum mass loss; n = 8 and 3, respectively. The PAML-31-1 phage release from HA-PEG gel data presented in (**h-j**) are referenced from the 10^{11} PFU/mL data in (**g**). Schematic in (**a**), (**d**) generated with BioRender. Data are presented as mean ± S.D for (**c**), (**e**), (**g**), (**h**), and (**j**).

PAML-31-1 phage effectively suppresses *Pa* in planktonic culture and on agar

As HP demonstrated the capability to deliver multiple *Pa* phages at high titres in a sustained manner, we next aimed to identify the most effective phage against *Pa* Xen41, a bioluminescent strain of *Pa* that could enable visualization of infection in a murine infection model. To this end, planktonic suppression assays (PSA) were conducted comparing the bioactivity of phages PAML-31-1, LPS-5, and Luz24, where the time evolution of optical density at 600 nm (OD600) of bacteria co-cultured with each of the phages was monitored.

PAML-31-1, which specifically targets lipopolysaccharide (LPS) in the outer membrane of *Pa*, showed the most substantial suppression of Xen41 among the tested phages. This was evidenced by a delayed onset of resistance and compression of the OD600 curve, which was quantified as the "Suppression Index" (SI%) (**Fig. 2a, b**) [65]. LPS-5, which also targets *Pa* LPS, demonstrated comparable efficacy to PAML-31-1 in the PSA. Subsequent tests of PAML-31-1 and LPS-5 involving different MOIs revealed that an MOI of 8,000 was necessary for effective suppression. Only this MOI achieved an SI% greater than 80%, without bacteria densities rebounding to the control level in 48 hours (**Supplementary Fig. 3a-d**). Of note, PAML-31-1 at MOI of 0.08 still achieved nearly 50% suppression. In contrast, bacterial densities were nearly unaffected by LPS-5 at MOI of 80 or below. These data indicate that PAML-31-1 is most effective against planktonic Xen 41 *Pa* among the tested phages.

Next, to contextualize the suppression capability of the phage released from HP encapsulating 10^{11} PFU/mL, we evaluated the SI% achieved by the amount of PAML-31-1 released HP each day. Remarkably, even on day 7, the PAML-31-1 released suppressed 30% of planktonic *Pa* despite a lower phage amount released that day (**Fig. 2c**). This prolonged suppression underscores the nonlinear nature of phage-bacteria interaction and the potential of HP to control bacterial burdens over extended timeframes *in vivo*.

HP disrupts *Pa* biofilms

We next examined how phage released from HP were effective in treating bacteria protected by biofilms. Biofilms are dense polymeric matrices that harbor both actively growing and dormant bacterial populations that are prevalent in chronic wounds [2,66], and can diminish the efficacy of antimicrobials and complicate treatment outcomes [67–71]. Fortunately, phages can penetrate bacterial biofilms [72]. To better predict bacteriophage activity against bacterial biofilms, we explored the efficacy of HP versus a control gel (a HA-PEG hydrogel free of phage), against bacteria immobilized on agar or grown as biofilms.

First, we assessed the efficiency of plaquing (EOP) of our set of phages against the luminescent *Pa* strain Xen41 compared to its parent strain, PAO1. PAML-31-1 showed less than a one-log reduction in EOP against Xen41 versus PAO1, whereas Luz24 was significantly less effective against Xen41 versus PAO1, showing three-log reductions in EOP (**Fig. 2d**). Notably, LPS-5 exhibited markedly reduced plaquing efficiency when assessed on agar plates than might be predicted based on its relatively stronger suppression of planktonic Xen41 compared to Luz24, with a six-log reduction in EOP. These findings hint that phages effective against planktonic bacteria may not exhibit the same efficacy against bacteria grown on a semi-solid substrate [73]. Consequently, we selected PAML-31-1 in our subsequent studies.

We then tested whether PAML-31-1 could still escape HP and lyse *Pa* grown on a semi-solid substrate, even when the hydrogel was not submerged in fluid as was assessed previously. To test this, we measured the zone of inhibition (ZOI) produced by HP relative to a control gel on Mueller-Hinton agar plates inoculated with *Pa*, with both gels placed on the plate without media added. HP caused a 60% increase in the area of ZOI relative to the control gel, indicating that phages could not only escape HP under drier conditions than previously tested, but also that they could infect and propagate beyond the area in direct contact with HP (**Fig. 2e, f**).

To assess the efficacy of PAML-31-1 against established biofilms, we inoculated PAO1-GFP on the surface of top agar in a multi-well plate, allowed biofilms to grow for 24 hours, and then treated the established biofilms either with PAML-31-1 added directly into the media, or with HP or a control gel in a transwell insert. Both PAML-31-1 and HP disrupted established biofilms, with reductions in biofilm thickness of 43% and 52% at 21 hours, respectively, relative to pretreatment. No disruption of biofilm growth was observed with the control gel or untreated control (**Supplementary Fig. 4a**). Furthermore, PAML-31-1 and HP decreased biofilm density by 57% and 65% respectively, whereas the control gel and untreated control exhibited increases in biofilm density of 55% and 72% (**Fig. 2g**). Confocal microscopy vividly illustrated the undisrupted densifying biofilm under treatment with control gel and untreated control and the marked to complete disruption under treatment with PAML-31-1 in media and HP (**Fig. 2h, i and Supplementary Fig. 4b**). Together, these results indicate that HP effectively suppresses and disrupts *P*a across planktonic and biofilm conditions.

PAML-31-1 most effectively suppresses Pa in planktonic culture and on agar

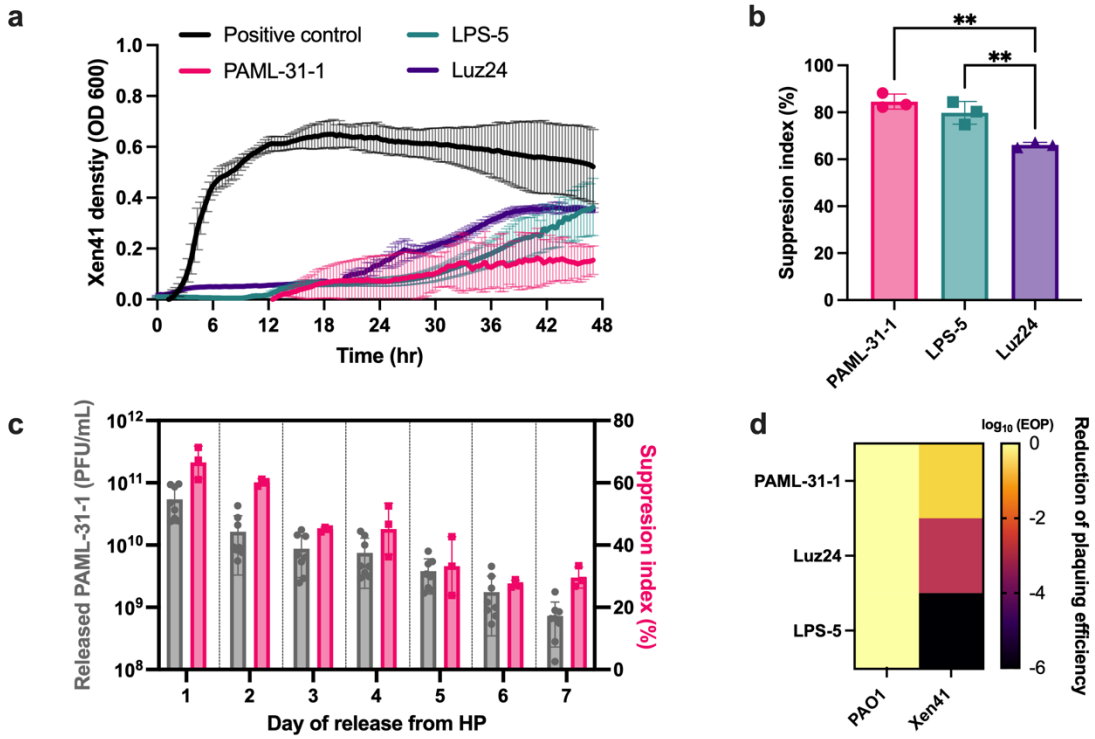

PAML-31-1 delivered from hydrogel effectively disrupts Pa biofilm

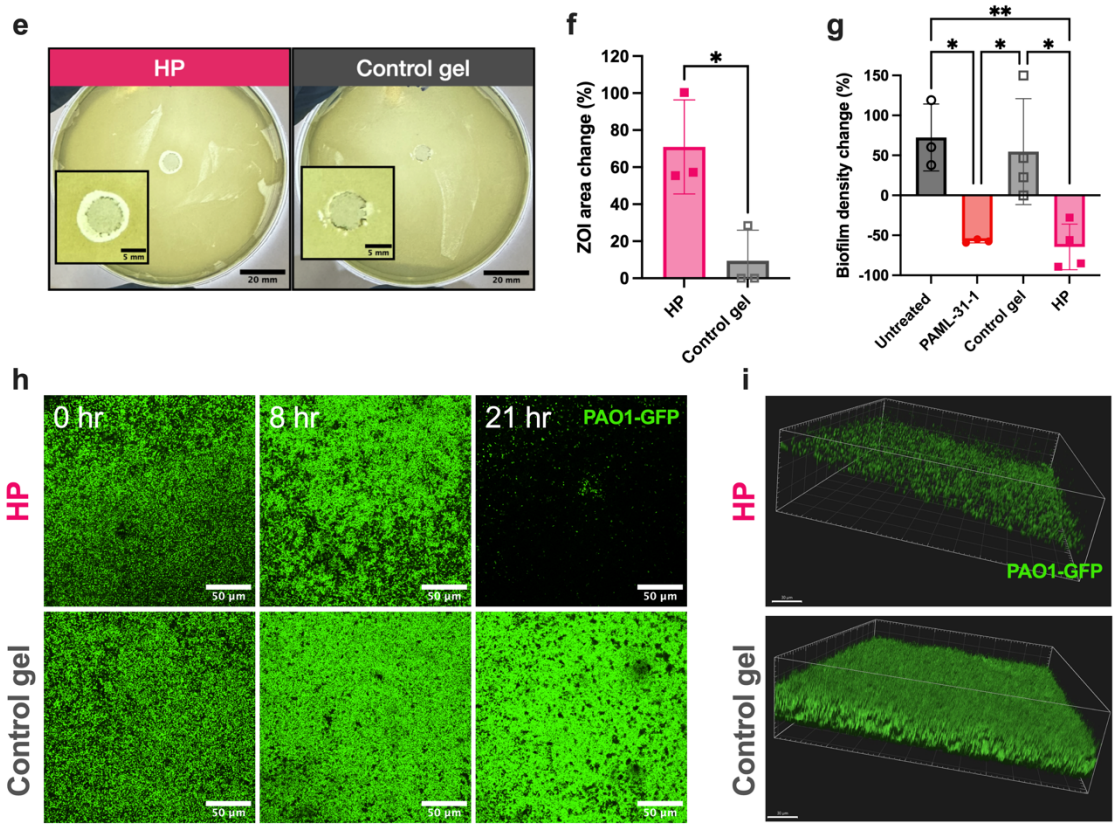

Fig. 2 High-dose PAML-31-1 delivered from HP is effective against *Pa* in planktonic and biofilm conditions. a,**b**, Three different phages—PAML-31-1, LPS-5, and Luz24—were co-cultured with *Pa* strain Xen41 in planktonic condition at the multiplicity of infection (MOI) of 8,000 with shaking for 48 hours and monitored every 20 minutes. Time evolution of optical density at 600 nm (OD600) (**a**), and the quantification of bacterial suppression by suppression index (SI%) (**b**); n = 9 for positive control and n=3 for each phage. **c**, Quantification of SI% of the titre of PAML-31-1 released from HP in transwell-release assay daily; n = 3 and 8, respectively. The daily released PAML-31-1 titer data are referenced from Figure 1g. **d**, The efficiency of plaquing (EOP) was quantified by comparing the log reduction of plaque counts of different phages on *Pa* strain Xen41 versus its parent strain PAO1; n = 1 each. **e**,**f**, The zone of inhibition (ZOI) formed by HP and control gel at 24 hours of gel placement on *Pa* lawn. The representative images of HP and control gel on *Pa* lawn (**e**), and quantification of change in ZOI area at 24 hours as a percent of initial area of hydrogel (**f**); n = 3 each. **g**,**h**,**i**, PAO1-GFP biofilm was formed on the surface of top agar and treated with untreated control, PAML-31-1 phage in media, control gel or HP for 21 hours; n = 3, 3, 4, and 4, respectively. The quantification of biofilm density changes (**g**), representative confocal images of biofilm incubated with HP and control gel treatments over hours (**h**), and the 3D rendering of biofilm at 21 hours (**i**). Scale bars: 20 mm for (**e**) and 5 mm for the inset, 50 μm for (**h**), and 30 μm for (**i**). Data are presented as mean ± S.D. One-way ANOVA with Tukey's post-hoc test for (**b**) and (**g**). Unpaired two-tailed Student's t-test for (**f**). (* $P \leq 0.05$, ** $P \leq 0.01$).

Murine chronic wound infection model with delayed treatment

We next investigated the *in vivo* efficacy of different phage treatment dosing and routes, including localized HP treatment, in a model designed to closely mimic the clinical parameters of wound care for patients with chronic wound infections. Thus, we developed a mouse PT model with delayed treatment. This model builds on our development of a chronic *Pa* wound infection model incorporating bacterial biofilms and chronic infection [74–76]. In contrast to other murine wound infection models, which introduce phage treatments within a few hours of or even along with bacterial inoculation, we delayed phage treatment to mice 24 hours post-infection (**Fig. 3a**).

We next identified the appropriate Xen41 inoculum required for a sustained infection. Mice were inoculated with a range of bacterial burdens from 1 x 10^5 CFU/wound to 3.7 x 10^6 CFU/wound. The mice were then assessed for whether they carried the infections after 24 hrs using *in vivo* bioluminescence imaging (BLI) to monitor the infection of PAO1-derived luminescent Xen41 and the efficacy of treatment daily. 5 x 10^5 CFU/wound represented the minimum inoculation dose that resulted in a 100% infection rate, and was therefore used as the inoculation dosage in experiments (**Fig. 3b, c**). Importantly, bacterial colony-forming units (CFU) correlated with luminescent flux *in vitro* (**Fig. 3d)** and *in vivo* (**Fig. 3e**). Despite the high infection rate, the model presented 100% mice survival (**Fig. 3f**) and minimal weight reduction of 5% over 6 days (**Fig. 3g**).

Localized phage delivery reduces bacterial burden in infected wounds

Prior to testing the efficacy of HP *in vivo*, we first investigated the general premise that phages delivered locally at sufficiently high titres could be effective in the treatment of infections. For these

studies, phages in solution were injected with a needle directly under a semi-occlusive dressing (Tegaderm) onto the wound bed (**Fig. 3h**). The Tegaderm here served to trap the fluid in place, thereby serving as a local reservoir of phage. While semi-occlusive dressings are typically not applied to exudative or infected human wounds because they can trap bacteria and contribute to tissue maceration, they were essential in this model to maintain wound infections, because they prevented the mice from physically removing the infection and treatments. We applied two different phage doses: a single high-dose (HD, 1 x 10^{11} PFU/mL, 40 uL) and a single low-dose (LD, 2.5 x 10^{10} PFU/mL, 40 uL) (**Fig. 3i**). We also delivered a regimen of daily low-dose phage for four days (DD, 2.5 x 10^{10} PFU/mL/day, 40 uL). Bacterial burden in wounds was monitored daily using BLI, where a bioluminescent flux signal below the limit of detection (LoD) was interpreted as the infection being cleared (**Fig. 3j**). At the end of the experiments, wound tissues were harvested, homogenized, plated, and counted for CFUs, to assess the remaining bacterial burden, and for PFUs, to assess active phage levels in the tissue.

We find that local treatment with phage was successful in reducing bacterial burden and eradicating infections compared to PBS controls. BLI data showed that treatment with phage significantly reduced bacterial burdens compared to PBS controls, with a substantial fraction of mice having their infections cleared (**Fig. 3j, k**). Notably, BLI data showed no significant differences between bacterial clearance in the setting of LD, HD, or DD dosing, though there was a trend favoring DD (**Fig. 3k**). Analysis of bacterial burden by culture-based characterization supported the conclusions derived from BLI. Comparing eradication rates did not demonstrate a significant difference between treatments but suggested a potential advantage of repeated phage exposure from DD, with 29% eradication rate versus 18% in the single high-dose group (HD) and 16% in the single low-dose group (LD) (**Fig. 3l**). Relative to PBS control treatment, mice treated with LD (n=19), HD (n=11), and DD (n=14) all presented significant bacterial burden reduction, with 1.44-, 2.16-, and 2.20-log reductions in CFU/mg at the end of the study, respectively **(Fig. 3m)**. Interestingly, the total amount of phage in the wound homogenate was similar between treatment groups, regardless of the differences in treatment dosage and frequency (**Fig. 3n**). Thus, these data indicate that local delivery of phage is effective at reducing bacterial burdens and eradicating infections in some mice. While these studies highlight the efficacy of local phage delivery, trapping a body of fluid over the wound for a week using a semi-occlusive dressing is likely not feasible in the setting of a human patient, motivating the use of HP.

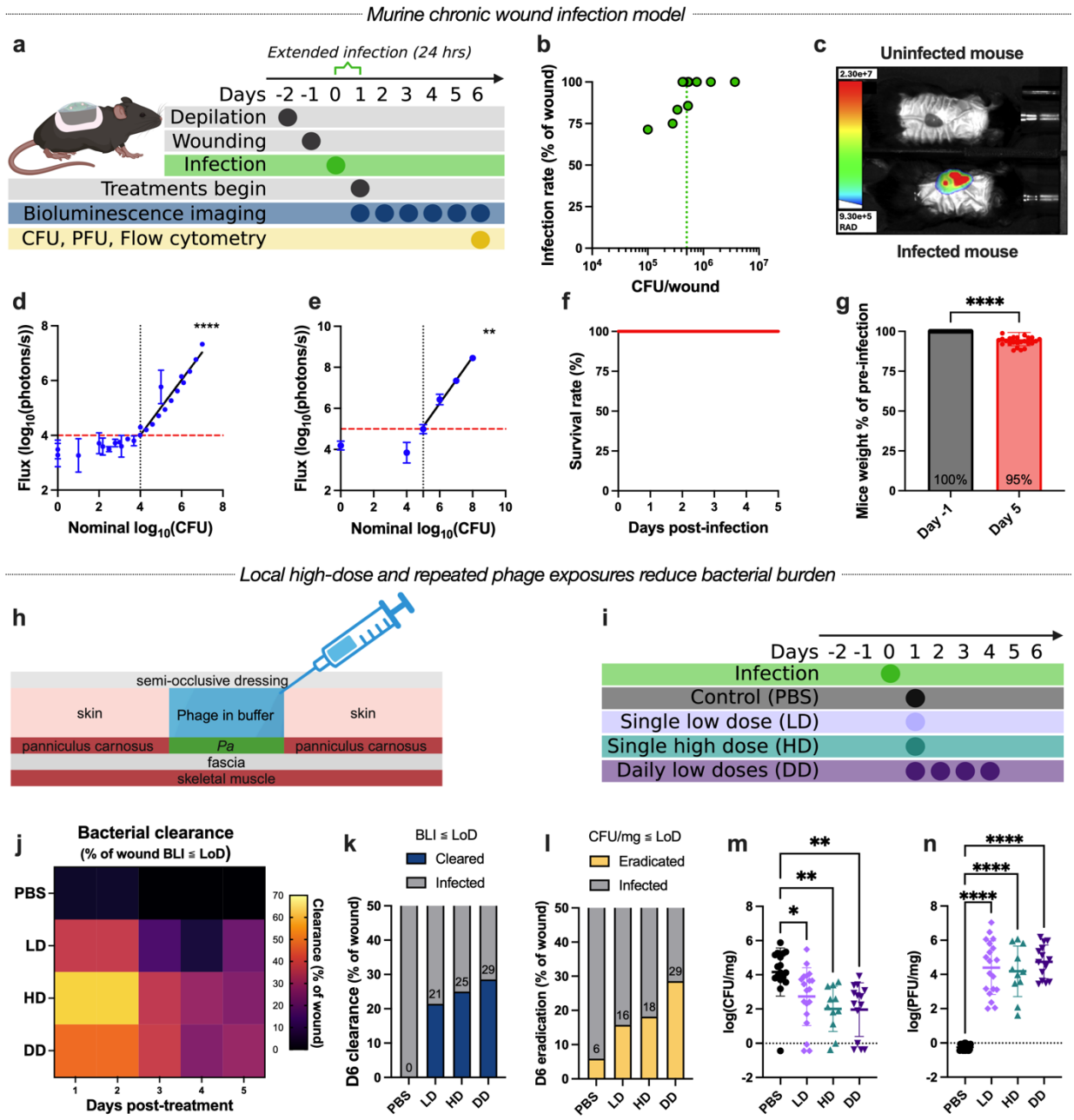

Fig. 3. High-dose and repeated local phage delivery reduce bacterial burden. a-g, Development of BLI and murine wound infection model**.** Illustration of the timeline of murine wound model (**a**); PAO1 Xen41 *in vitro* luminescent signal and nominal CFU correlation; the wound infection rate at different inoculation density of Xen41 (**b**); the representative BLI image of uninfected (top) and infected (bottom) mice, where color bar indicates the flux intensity (**c**); the PAO1 Xen41 *in vitro* (**d**) (Pearson r = 0.953, P < 0.001); R^2 = 0.889) and *in vivo* (**e**) (Pearson r = 0.996, P = 0.0043; R^2 = 0.977) luminescent signal and nominal CFU correlations; mice survival rate after inoculated with 5 x 10^5 per wound PAO1 Xen41 up to 5 days post-infection (**f**), n = 20; and the percentage of weight to pre-infection weight for mice on Day 5 after inoculation with 5 x 10^5 per wound PAO1 Xen41 (**g**), n = 29; **h**, Illustration demonstrates how mice receive liquid phage treatment by topical injection under Tegaderm dressing. **i**, Illustration of the murine wound

study to compare the efficacy of PT with different dosing concentration and frequency. **j**, **k**, The real-time monitoring of bacterial burden with BLI. The heatmap presents the daily calculated percentage of wound infection clearance, defined as bioluminescent flux lower than the limit of detection (LoD) (**j**), and the percentage of wound infection clearance at the end of the study, day 5 post-treatment (**k**); n=17 for PBS, n=14 for LD, n=12 for HD, and n=14 for DD. **l**,**m**,**n**, Endpoint characterization of harvested mice wound tissue. The eradication rate defined as the percentage of wounds having bacterial burden below LoD (**l**), and bacterial burden (CFU/mg) (**m**) and phage counts (PFU/mg) (**n**) recovered; n=17 for PBS, n=19 for LD, n=11 for HD, and n=14 for DD. Schematic in (**a**), (**h**) and (**i**) were generated with BioRender. Data are presented as mean ± S.D. Unpaired two-tailed Student's t-test for (**g**). One-way ANOVA with Tukey's post-hoc test for (**m**) and (**n**) (* $P \leq 0.05$, ** $P \leq 0.01$, **** $P \leq 0.0001$).

Localized HP clears wound infection more effectively than systemic phage administration

Next, we evaluated the efficacy of HP in treating infections compared to systemic (intravenous) phage administration. We hypothesized that localized phage treatment would enhance the clearance of infection from wounds compared to systemic treatment. To test this, mice were treated with HP or PBS as topical injections under a layer of Tegaderm (**Fig. 4a, b)**, or with IV injection of the same total amount of phage (**Fig. 4c**). Daily BLI measurements indicate that HP was superior to treatment of IV phage injection (**Fig. 4d**). Mice treated with HP had a 40% clearance rate at the end of the study on day 5 post-treatment, compared to a clearance rate of just 6% for mice treated with IV injection of phage (**Fig. 4e**). The eradication rate derived from culture-based assay demonstrated similar improvement in HP relative to IV as the BLI measurements: HP treatment eradicated 25% of infections in mice, compared to just 5% for IV treatment (**Fig. 4f**). HP demonstrated far superior antimicrobial efficacy compared to IV and PBS control, with a >2-log reduction in CFU/mg wound tissue relative to PBS for HP-treated mice (2.15, n=20) compared to a <1-log reduction in CFU/mg for IV-treated mice (0.72, n=20) (**Fig. 4g**), despite that similar amounts of phages were found in the wound homogenates in HP- and IV-treated mice (**Fig. 4h**).

Together, our results indicate that the localized delivery of phages via HP results in superior burden reduction and eradication of *Pa* from murine wounds than systemic therapy. These data point to the merit of sustained delivery of high-titre phages locally via hydrogels.

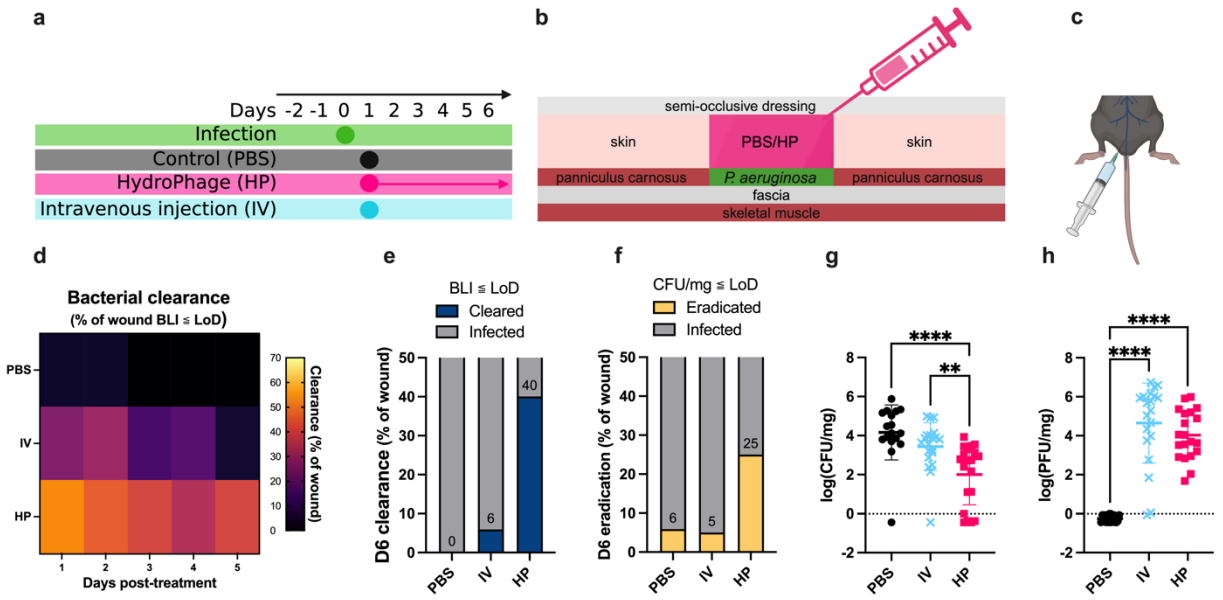

Fig. 4. Localized HP treatment clears infection from murine wounds. a, Illustration of a murine wound infection study to test the efficacy of HP and IV phage injection treatments. **b**, Illustration demonstrates how mice receive HP or PBS control treatment by topical injection under Tegaderm dressing. **c,** Illustration demonstrates the penile vein injection for IV phage treatment. **d**,**e**, The real-time monitoring of bacterial burden with BLI. The heatmap presents the daily calculated percentage of wound infection clearance, defined as bioluminescent flux lower than the LoD (**d**), and the percentage of wound infection clearance at the end of the study, day 5 post-treatment (**e**); n=17 for PBS, n=17 for IV, and n=15 for HP. **f**,**g**,**h,** Endpoint characterization of harvested mice wound tissue. The eradication rate defined as the percentage of wounds having bacterial burden below LoD (**f**). and bacterial burden (CFU/mg) (**g**) and phage counts (PFU/mg) (**h**) recovered; n=17 for PBS, n=20 for IV, and n=20 for HP. Schematic in (**a**) and (**b**) were generated with BioRender. Data are mean ± S.D. One-way ANOVA with Tukey's post-hoc test for (**g**) and (**h**) (** $P \leq 0.01$, **** $P \leq 0.0001$).

Successful HP treatment partially restores the local inflammatory environment in the skin

We next assessed the local immunologic response to *Pa* wound infection and how this was altered by HP treatment. The abundance of myeloid and adaptive immune cells in the skin at the end of the infection study were quantified. A flow cytometry panel with 13 labels (**Supplementary Table 1**) was used to discriminate most major myeloid and adaptive cell populations in the skin. After gating on singlet, live, and $CD45^+$ cells, we quantified the abundance of natural killer (NK) cells, neutrophils, macrophages, B cells, and T cells, and excluded monocytes, monocyte-derived dendritic cells (MoDCs), and conventional dendritic cells (cDCs) using the gating strategy shown in **Supplementary Fig. 5**. Apart from NK cells, subpopulations of innate lymphocytes were not discriminated in the downstream gating.

Infection with *Pa* caused several robust changes to the immune cell composition of mouse wounds on day 6 post-infection. We observed a significantly increased proportion of $CD45^+$ cells and natural killer cells, and a trend towards increased neutrophils. We also observed a significant reduction in the proportion of T cells, but no changes in the abundance of skin-associated B cells **(Fig. 5a)**. Successful treatment with HP was partly able to reverse these effects, with decreases in $CD45^+$ cells, NK cells, and neutrophils following successful eradication of bacteria **(Fig. 5b)**. Thus, immune profiling shows several infection-dependent changes in the abundance of skin-associated immune cell populations and that successful treatment with HP can revert some of those changes.

Finally, we conducted toxicologic studies to assess the biocompatibility and immunogenicity of the HA-PEG hydrogel and PAML-31-1 phage *in vitro*. We cultured monolayers of RAW264.7 murine macrophage-like cells and incubated the monolayers for 24 hours at 37°C with the HA-PEG hydrogel in transwell inserts (**Fig. 5c**). We found that neither the HA-PEG hydrogel nor PAML-31-1 exhibits any cytotoxicity to RAW264.7 cells (Fig. 5d). We also used flow cytometry to assess if the HA-PEG hydrogel polarized RAW264.7 cells towards M1 or M2 phenotypes, by measuring expression of canonical M1 (CD80, CD86) or M2 (CD163, CD209) markers. We found no upregulation of these markers in response to treatment with the HA-PEG hydrogel (**Fig. 5e-h**).

Overall, these data suggested that the HA-PEG hydrogel is biocompatible and nonimmunogenic to macrophage-like cells, further supporting the suitability of HP for use *in vivo*.

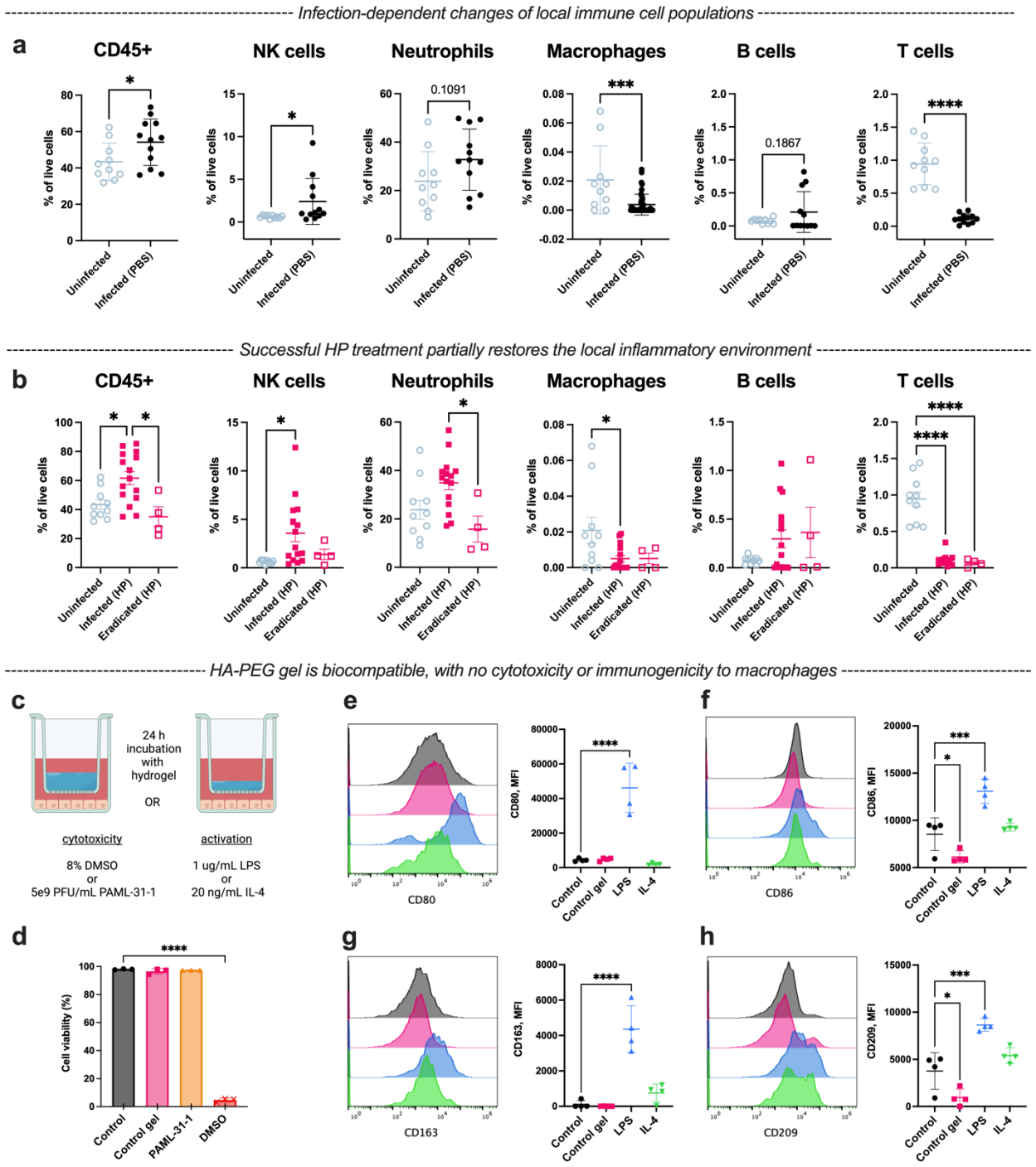

Fig. 5. Flow cytometry shows infection-dependent changes and eradication-dependent reversal of skin-associated immune cell populations with HP. **a**, The abundance of CD45^{+}, natural killer (NK) cells, neutrophils, macrophages, B cells, and T cells in uninfected mouse wounds versus wounds infected with *Pa* and treated with PBS; n = 10 for uninfected mice and n = 12 for infected (PBS treated) mice. **b**, The abundance of CD45^{+} cells, NK cells, neutrophils, macrophages, B cells, and T cells in uninfected mice wounds versus mice treated with HP, where the treatment results were stratified by outcome as either infected or eradicated; n = 10 for uninfected mice, n = 15 for infected (HP treated) mice, and n = 4 for eradicated (HP treated) mice.

See Supplementary Fig. 6 for gating strategy and cell definitions. **c**, Schematic of transwell exposure assay of cytotoxicity and macrophage activations. **d**, Cytotoxicity of HA-PEG gel (control gel) and PAML-31-1 phage to RAW264.7 cells using transwell system; n = 3 each. **e**-**h**, Representative histograms (left) and median fluorescence intensity (MFI) of fluorochrome-conjugated antibodies against classical M1 (CD80, CD86) and M2 (CD163, CD209) markers in RAW264.7 cells after treatment with media only control, control gel in transwell system, 1 ug/mL *E. coli* LPS, or 20 ng/mL mIL-4; n = 4 each. Data are mean ± S.D. Unpaired two-tailed Student's t-test for (**a**). Ordinary one-way ANOVA with Tukey post-hoc tests for (**b**) and with Dunnett post-hoc tests for (**d**-**h**) (* $P \leq 0.05$, *** $P \leq 0.001$, **** $P \leq 0.0001$).

Development of PAML-31-1 resistance is independent of treatment dosage, route, and efficacy

While phages in the context of HP and DD are more successful at eradicating infections, the eradication rates did not exceed 30%. We hypothesized that bacteria might develop resistance against phages *in vivo* if not fully eradicated, similar to the behavior observed in the PSA (**Fig. 2a and Supplementary Fig. 3a, c**). The positive correlation between phage and bacteria counts at the endpoint suggested that persisting bacterial burdens were not due to phage depletion (**Fig. 6a**).

To confirm that resistance to PAML-31-1 had developed *in vivo* in response to phage treatments, we conducted a PSA that re-challenged the stationary phase bacterial isolates from previous *in vivo* treatment regimens with PAML-31-1 (**Fig. 6b**). Bacterial isolates from all phage treatment groups exhibited significant reductions in SI% compared to phage-unexposed wild-type Xen41 and PBS control groups, indicating that substantial resistance had developed even with ineffective treatments such as IV injection (**Fig. 6c, d**). The comparable SI% among resistant isolates suggests that the level of resistance was independent of the treatment efficacy.

To summarize, these results demonstrated that resistance against PAML-31-1 developed regardless of treatment dosage, frequency, delivery route, and was not correlated with the reduction of bacterial burden.

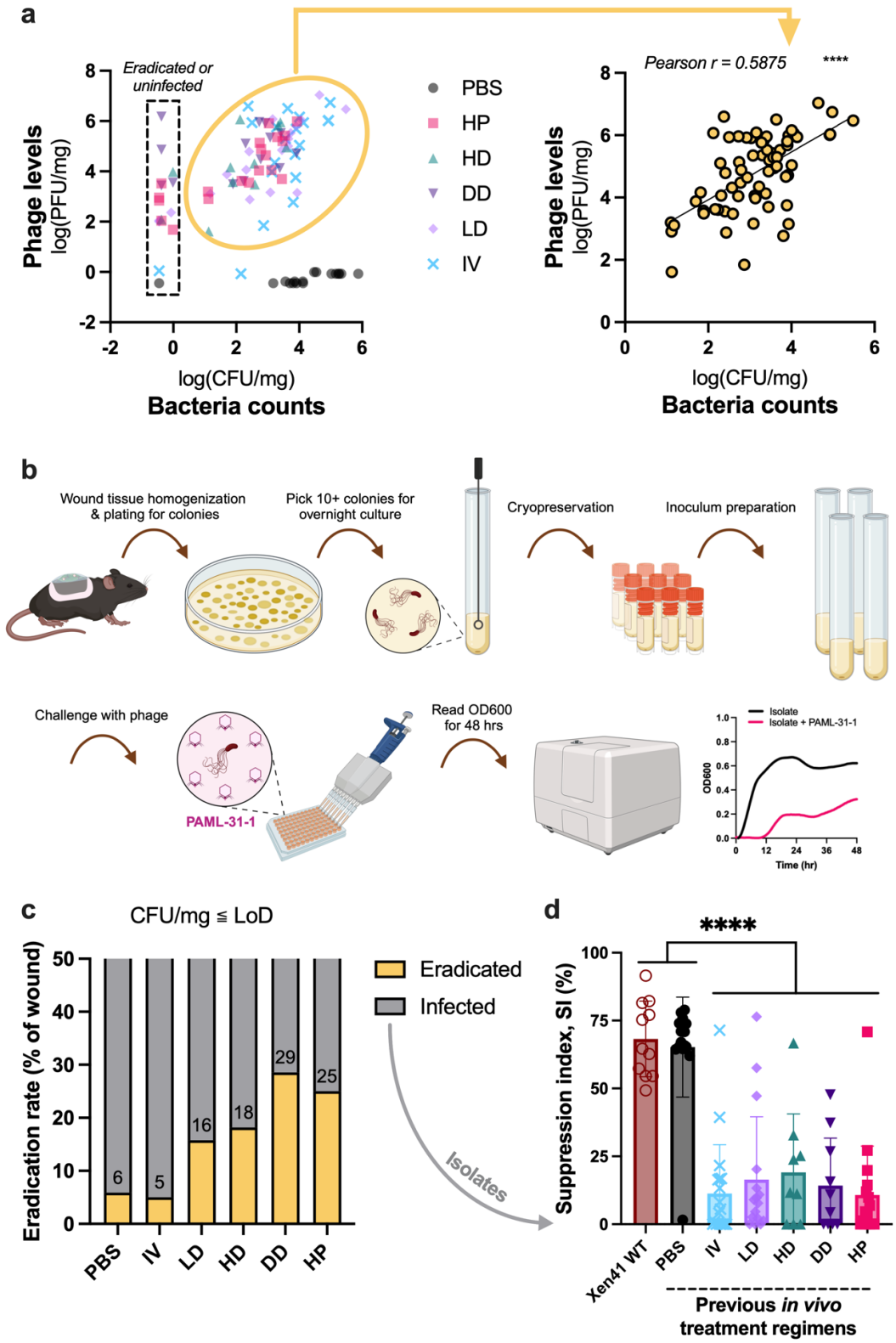

Fig. 6. Development of phage resistance from phage treatment is independent of treatment, dosing, route, and efficacy. a, The endpoint phage counts recovered from mice wounds were

plotted against the bacteria counts recovered (left). The dotted box encircles the wounds that did not have bacteria counts, either from eradication or not infected. The correlation of log-transformed PFU/mg to CFU/mg for the wounds that had both phage and bacteria recovered (right); n = 68. Two-tailed Pearson correlation coefficient r = 0.5875 (**** $P \leq 0.0001$) and R^2 = 0.3452. **b,** Schematic of PSA for the mice wound isolates to characterize bacteria resistance after prior PAML-31-1 treatment regimens, compared to PBS-treated control and wild-type Xen41. **c,** Summary of eradication rates by phage treatments investigated from Figures 3i and 4f, with the gray arrow indicating the portion (endpoint infected) of wound isolates for downstream resistance characterization. **d,** Quantification of SI% for PAML-31-1 against Xen41 WT and wound isolates with previous *in vivo* treatment regimens; n = 11 for Xen41 WT, n=15 for PBS, n=19 for IV, n=16 for v, n=9 for HD, n=10 for DD, and n=16 for HP. Schematic in (**b**) was generated with BioRender. Data are mean ± S.D. One-way ANOVA with Tukey's post-hoc test (**** $P \leq 0.0001$).

Discussion

This study reported the development of HydroPhage (HP), a hydrogel crosslinked with both CC and DCC and engineered for the sustained delivery of phages. The use of HP demonstrated superior bacterial eradication through localized, high-concentration, and sustained phage delivery compared to IV injection in a preclinical murine wound model of chronic infection. Analysis of host responses indicates the partial restoration of the local inflammatory environment following successful HP treatment, and the biocompatibility of HP. However, we found that the rise of phage resistance limits the overall efficacy of monophage therapy broadly, regardless of treatment dosing and routes. Nonetheless, these data highlight the significant potential of hydrogels in treating chronic wound infections, particularly given the increasing prevalence of MDR pathogens like *Pa*.

The underlying innovation of this study is a hydrogel that releases phage in a sustained manner. Previous hydrogel- or microparticle-based approaches often present either rapid burst release [56,60,77–80] or low recovery of phage without mechanical (e.g., shaking) or biochemical (e.g., protease activity) interventions [57,58,81]. Due to their intrinsic viscoelasticity, injectability, and self-healing characteristics, DCC hydrogels have gained significant attention in many biomedical applications [60,82–84]. Among various DCC chemistries considered, hemithioacetal crosslinking is ideal for making hydrogels for topical application, as the rapid kinetics and high reversibility provide immediate enhancement of viscosity and shear-thinning behavior [85]. We thus leveraged these properties from hemithioacetal crosslinks combined with the stability of covalent thioether bonds, to develop an adherent slow-gelling HA-PEG hydrogel. The low covalent thioether crosslink density provides the necessary stability without trapping sub-micron scale particles, making the gel susceptible to slow erosion and thereby enabling sustained release of phages out of hydrogel. Further, HP is easily injectable and can fill in the contour of the uneven wound bed to provide prolonged contact with the affected area. To our knowledge, this is the first introduction of a hydrogel that shows sustained release of phage at high titres (i.e. $>10^9$ PFU/ml gel) over a week without the need of mechanical or biochemical interventions.

We adapted a murine chronic wound infection model to provide a suitable framework to assess PT in wounds. In previous models of PT, phages are co-delivered with bacteria, which may not allow the infection to take hold, whereas our model gives one day for the infection to develop. We also utilized *in vivo* bioluminescence imaging to monitor the daily progression of infections in conjunction with gold-standard culture-based assays to examine the bacteria count at the end of the study. Thus, this model provides unique insight into resistance dynamics throughout the treatment course with paired endpoint analyses.

Our results establish the advantage of localized phage delivery over IV for treating wound infections. It is a common understanding that topical phage treatment may be a safer, cost-effective, and convenient route of administration for wound infection compared to IV [30,40]. However, improved efficacy of topical versus IV treatment of PT has not been shown previously. IV phage could be rapidly cleared by the liver and spleen rather than the induction of neutralizing antibodies, given the time frame of our study [86,87]. Our BLI results show that inferior bacterial suppression starts in the early days post-treatment. Hence, the ineffectiveness of IV is potentially the result of a low effective concentration of active phage delivered to the site of infection [33,88]. Surprisingly, PFU levels at the endpoint are similar from local versus systemic administration, suggesting phage levels catch up via *in situ* propagation, but not before phage resistance in the infection develops.

Our chronic wound infection model suggests that higher concentrations of phages and more frequent dosing may be beneficial. Notably, though differences were not significant, we observed a trend towards better efficacy of daily phage dosing (DD) and HP compared to a single dose (LD), with a greater reduction of bacterial burden and higher eradication rate. These data are consistent with the benefits reported for repeated treatment in numerous case studies [40].

Our results also highlight the challenge of phage resistance in PT. In clinical cases and animal models of PT, phage resistance was often not quantitatively examined nor even reported [39,89]. We observe significantly reduced phage susceptibility of bacteria isolated from infected mice wounds, indicating the rise of phage resistance in a short period of time. Surprisingly, this was observed under all conditions, including IV treatment, which was ineffective in reducing bacterial burdens. This complexity of phage-host interaction *in vivo* highlights the limitations of phage monotherapy, which could potentially be overcome by phage cocktail treatments [90]. Nonetheless, our result underscores the importance of maintaining high local phage concentration and frequent dosing to manage wound infection efficiently before the emergence of phage resistance. It also implies the potential benefits of monitoring phage susceptibility quantitatively early on, before the relapse of infection.

We show that HP is well-tolerated and non-inflammatory, supporting the established notion that PT is safe. Recent studies have highlighted the involvement of natural killer (NK) cells in responding to bacterial infections, including directly eradicating pathogens such as *Pa* [91–94]. Indeed, HP treatment was associated with reduced NK cells and neutrophils to levels comparable to those in uninfected wounds, suggesting a resolution of inflammation. The short duration of our model likely limits the activation of adaptive immunity, which is evident from the relatively low percentage of B cells and T cells. The unexpected persistent reduction in T cell levels post-successful bacterial eradication suggests a potential mechanism, such as premature apoptosis induced by bacterial products[76], warranting further investigation. Overall, the phage treatment does not exacerbate inflammation post-infection and successful bacterial eradication reduces inflammation, supporting the safety of PT, as has been previously demonstrated [44,45,95,96]. Thus, this work establishes the great potential of localized phage delivery with hydrogels in treatment of MDR infection.

Limitations of this study include: 1) With its 100% survival rate, our model did not include mortality outcomes, which could provide further insights into the trade-off between bacteria virulence and phage resistance. 2) Clinically, patients exhibit a wide spectrum of wound severity and exudate levels, making it uncertain whether the localized HA-PEG hydrogel will perform consistently under variable conditions. 3) The study primarily focused on bacterial burden control; thus, phage treatments' impact on wound healing was not elucidated. 4) This study relied on a single strain of *Pa* and a single phage for the murine model. 5) The use of Tegaderm is essential in this model to maintain infections and deliver topical liquid phage; however, they are unsuitable for use in grossly infected, substantially exudative, or deep wounds [97–99]. This limitation highlights the potential advantage of leveraging hydrogels to provide prolonged phage contact with infected wounds.

Methods

Phage propagation

Phages were propagated using methods previously established in the lab [100]. PAML-31-1, LPS-5, Luz24, and OMKO1 were propagated in *Pseudomonas aeruginosa* (*Pa*) strain PAO1. Early- to mid-log phase cultures were infected with phages to generate lysates from 300 mL cultures.

Phage purification using AKTA-FPLC system

Bacteria were removed by 2-3 rounds of centrifugation at 8000 x *g*, 10 min, 4°C. Supernatants were filtered through a 0.22 µm polyethersulfone (PES) membrane filter (Corning, Cat. No. 4311188). The supernatant was treated with 5 U/mL Benzonase Nuclease (Sigma-Aldrich, Cat. No. E8263) overnight to digest free DNA. Benzonase-treated lysates were then mixed with 3M KH_2PO_4 buffer (pH 7.0) in a 1:1 ratio in preparation for purification by fast protein liquid chromatography (FPLC). The FPLC-based virus purification was conducted with a CIMmultus OH 1 mL monolithic column with a 2 µm channel size (Sartorius BIA Separations, Ajdovščina, Slovenia). The washing, regeneration, performance test, and storage of the column was carried out according to manufacturer recommendations. The column was attached to an ÄKTA Pure FPLC (GE Healthcare Biosciences, Sweden) equipped with a P960 sample pump and analyzed with UNICORN 5.0 software (Cytiva Life Sciences, USA). All purification protocols were run at room temperature and all buffers and samples were filtered through a 0.22 µm PES membrane. 40-60 mL of the mixed sample was loaded onto a pre-equilibrated column with 1.5 M KH_2PO_4 loading buffer, pH 7.0. After sample loading, the column was washed with 10 column volumes of loading buffer to remove unbound particles. The elution of bacteriophage was performed using a linear gradient over 20 column volumes from 1.5 M to 20 mM KH_2PO_4. The fraction corresponding to the eluted phage was collected based on UV A280 measurement. We then dilute or perform buffer exchange on the eluted phages into Tris+Mg buffer (100 mM NaCl, 50 mM Tris-HCl, 8 mM $MgSO_4$, pH 7.50).

Phage characterization

The size and morphology of phages were assessed using transmission electron microscopy (TEM) on a JEOL JEM1400 (JEOL USA Inc., Peabody, MA, USA) operating at 80 kV. In brief, 5 µL of diluted phage solution was applied onto carbon-coated copper grids (FCF-200-Cu, Electron Microscopy Sciences, Hatfield, PA, USA). Following a 3-minute incubation, the grid was immersed in ddH2O and subsequently treated with 1% uranyl acetate for staining. After drying for 15 minutes, the sample was ready for TEM imaging.

Hydrogel preparation

For making HA-PEG hydrogel, thiolated hyaluronic acid (HA-SH, 450 kDa, Blafar Ltd), hyperbranched PEG multi-acrylate (HBPEG, 10 kDa, Blafar Ltd), 4-arm PEG-aldehyde (4ALD, 10 kDa, CreativePEGWorks), and 4-arm PEG-benzaldehyde (4BLD, 10 kDa, SINOPEG) were reconstituted in PBS+Mg (Phosphate-Buffered Saline + 8 mM $MgSO_4$, pH=7.50) at concentration of 1wt%, 5wt%, 40 mM, and 40 mM respectively, adjusted to neutral pH, purged with argon gas and kept on ice before use. Appropriate volumes of the following reagents were added into an Eppendorf tube in the order of: PBS+Mg, HBPEG, 4-BLD, 4-ALD to make a crosslinker mixture. Next, phage was added to the crosslinkers and vortexed, then HA-SH was added, vortexed, and mixed thoroughly by pipetting. The viscous slow-gelling mixture then could be withdrawn by pipette to deposit into transwell insert (Corning, USA, Cat. No. 353492) for *in vitro* assays or by

insulin syringe with 28G needle (BD, REF. 329461) to inject for *in vivo* treatment. The final formulation of HA-PEG hydrogel was 5 mg/mL HA-SH, 1 mg/mL HBPEG, 75 mg/mL of 4-arm PEGs with 10% 4BLD and 90% 4ALD, and 10^{11} PFU/mL phage unless otherwise noted.

For making ionically crosslinked alginate hydrogel (AG-Ca^{2+}), lyophilized alginate (PRONOVA UP VLVG, IFF, USA) was reconstituted in Tris+Mg buffer (50 mM Tris-HCl, 100 mM NaCl, 8 mM $MgSO_4$) at 4wt%. Calcium sulfate was prepared as a form of saturated slurry in deionized water at 500 mM. Reconstituted alginate and phage solution were added to a 1 mL syringe, and calcium slurry was added into another syringe using pipette. The solution in each syringe was thoroughly mixed by moving the plunge up and down, before connecting syringes with a Luer lock. Alginate, calcium, and phages were then mixed thoroughly between syringes, then deposited 100 uL onto a transwell insert. The formulation of AG-Ca^{2+} hydrogel was 2wt% alginate, 50 mM calcium, and 10^{11} PFU/mL phage. Detailed polymer information was included in Supplementary Table 3.

Transwell-release assay

Transwell inserts for 24-well plates were blocked in a solution of 2% bovine serum albumin (BSA) in PBS for 1-2 hours, rinsed with PBS+Mg for 10 min, then thoroughly aspirated then air-dried prior to use (20 min, covered, room temperature). 100 uL of hydrogel with encapsulated phage was aliquoted to each transwell insert and incubated in a closed box at room temperature for 3-3.5 hours until the hydrogels had fully gelled. After gelation, transwells were transferred to 24-well tissue culture-treated plates (Corning, NY, USA, Cat. No. 3524) containing 500 uL of PBS+Mg buffer. An additional 200 uL of PBS+Mg was added on top of the hydrogel to prevent drying. After 24 hours of incubation at 37°C, the transwell insert with hydrogel was removed. The buffer on top of the hydrogel and any residual buffer on the bottom of the transwell were carefully removed and combined with the buffer in the 24-well plate and stored at 4°C for phage titre quantification. The transwell was transferred into a new well containing 500 µL of fresh buffer, and 200 µL of fresh buffer was added on top. This process was repeated for 7 days.

HA-PEG hydrogel erosion

The erosion study on HA-PEG hydrogel without the phage encapsulation was performed by forming hydrogels in the transwell insert and submerged in the PBS+Mg buffer, transferred daily as described in the transwell-release assay method section. The dry mass of the hydrogel was weighed at each time point after the hydrogel was lyophilized. Erosion, defined as the percentage to maximum polymer mass loss, was quantified as the loss of dry mass at each time point normalized to the endpoint of the assay on day 7.

Plaque assays

Phages were enumerated by plaque assays using the spot dilution double-agar overlay technique. 100 µL of mid-log phase bacteria was added to 5 mL of top agar (5 g/L agar, 10 g/L tryptone, 10 g/L NaCl, 20 mM $MgSO_4$, 20 mM $CaCl_2$) and poured onto LB-agar plates to solidify. 10-fold serial dilutions of phages were prepared in 96-well polystyrene U-bottom tissue culture-treated plates (ThermoFisher Scientific, Waltham, MA, USA, Cat. No. 168136) in SM buffer (50 mM Tris-HCl, 100 mM NaCl, 8 mM $MgSO_4$, 0.01% gelatin (Sigma-Aldrich, USA, Cat. No. G7041), pH = 7.50). 10 µL of each dilution was spotted onto the top agar, incubated at 37°C overnight, and plaques were counted.

Planktonic suppression assay (PSA)

Overnight cultures directly from glycerol stock of Xen41 or cryopreserved mice wound isolates were prepared. 50 uL of diluted overnight culture of bacteria in "modified-LB" (LB buffer + 50 mM Tris-HCl + 8 mM $MgSO_4$, pH = 7.50) were prepared at the concentration of 3.75 x 10^7 CFU/mL in a 96-well plate. 100 uL of phages in modified-LB were aliquoted to the 96-well with bacteria to reach the target MOI in a total volume of 150 µL, topped with 15 µL of mineral oil to prevent evaporation, and covered with a gas-permeable sealing membrane (USA Scientific, Cat. No. 9123-6100). The final co-cultures were then incubated at 37°C in an automated spectrophotometer (Biotek Synergy 2, Agilent Technologies, USA) for 48 hours, with 5 seconds of shaking before OD600 was read every 20 min. The control was bacteria incubated with modified-LB instead of phages. Each sample was prepared in triplicates. The Suppression Index (SI%) was calculated from the formulation below to quantify the relative suppression of bacterial growth between phage-treated and non-treated condition [65].

$$Suppression\ Index\ (\%)\ =\ \frac{AUC_{48h}\ non\text{-}treated\ -\ AUC_{48h}\ phage\text{-}treated}{AUC_{48h}\ non-treated}$$

$$AUC\ =\ area\ under\ the\ curve$$

To evaluate the efficiency of different phages to suppress planktonic Xen41, an MOI of 8,000 was compared. For suppression of mice isolates by PAML-31-1 phage to evaluate resistance, an MOI of 500 was used.

Zone of inhibition (ZOI) assay

The subculture of overnight PAO1 culture at OD600 of 0.65 was dropped and spread onto a Mueller-Hinton agar plate and air-dried. 100 uL of HA-PEG hydrogel (5 mg/mL HA-SH, 1 mg/mL HBPEG, 75 mg/mL of 4-arm PEGs with 10% 4BLD and 90% 4ALD, and 10^{11} PFU/mL PAML-31-1 phage) were pre-formed and transferred to the inoculated agar plate after 3.5 hours of gelation. The hydrogel was allowed to seal with the agar surface for 15 min, before inverting and incubating at 37°C for 24 hours. The zone of inhibition (ZOI) was measured.

***In vitro* biofilm assay and confocal microscopy**

The overnight culture of PAO1-GFP was diluted to OD600 of 0.05 in tryptic soy broth (TSB) and kept on ice. 250 uL of top agar was solidified in each glass bottom 24-well plate (Cellvis, USA, Cat. No. P24-1.5H-N) before adding 300 uL of inoculum. The inoculum was allowed to adhere for 30 min in the incubator at 37°C, then the media was gently replaced with 500 uL of TSB. After 5 hours, each well was replaced with 800 uL of fresh TSB and then incubated overnight. At 24 hours, each well was gently rinsed with 800 uL of PBS+Mg, then replaced with 300 uL of modified-LB, followed by adding treatments. The control treatment was 200 uL of PBS+Mg, and phage treatment was 200 uL at 10^{11} PFU/mL, added directly into wells. Control gel treatment was 100 uL of HA-PEG gel in transwell insert topped with 200 uL of PBS+Mg, and HydroPhage (HP) treatment was 100 uL of HA-PEG gel containing PAML-31-1 at 10^{11} PFU/mL in a transwell insert topped with 200 uL of PBS+Mg. Biofilm was monitored with a laser-scanning Leica SP8 confocal microscope with 25x 0.95-NA water immersion objective at 0, 3, 8, and 21 hours. Media was not removed or replaced in between imaging time points to minimize the disturbance of biofilm and hydrogels. Biofilm density was quantified as the percentage of area with PAO1-GFP signal at the

base of biofilm, the biofilm and agar interface, and biofilm density change was defined as the change of biofilm density at 21 hours normalized to the initial density of each sample. Due to the significant presence of planktonic bacteria in the background above biofilm and/or the significant disruption of biofilm from treatments, the biofilm thickness was manually defined from the biofilm and media boundary to the base of biofilm determined from x-z and y-z projections. 3D rendering of the biofilm was reconstructed with Imaris imaging software (Oxford Instruments).

In vitro cytotoxicity and activation of hydrogel against RAW264.7 macrophages

A transwell exposure assay was used to measure the cytotoxicity and immunogenicity of pre-formed hydrogels against RAW264.7 murine macrophage-like cells (**Supplementary Fig. 6a)**. RAW264.7 cells were grown to passage 6 post-thaw in complete DMEM (DMEM/F12 + 10% fetal bovine serum + 1% penicillin/streptomycin). 5 x 10^4 cells were seeded in 24-well tissue culture-treated plates. After overnight incubation, the media was replaced with 500 µL of fresh cDMEM. Cells were treated for 24 h with media only (control), 8% DMSO (positive cytotoxicity control), 1 µg/mL *Escherichia coli* lipopolysaccharide (M1 polarizing positive control; Sigma-Aldrich, Cat. No. L3024-5mg), 20 ng/mL mouse IL-4 (M2 polarizing positive control; ThermoFisher Scientific, USA, Cat. No. 214-14-1MG), FPLC-purified PAML-31-1 at 5 x 10^9 PFU/mL, or 100 µL hydrogels in transwell inserts, with 200 µL of fresh media on top of the hydrogel to prevent drying. After 24 h incubation, media was removed and cells were rinsed once in PBS and stained with 300 µL of 1:3000 IRDye 800CW in PBS for 15 minutes at room temperature. Staining was quenched by the addition of 1 mL ice-cold FACS buffer. After centrifugation, cells were resuspended in 300 µL of anti-mouse CD16/32 (Fc block) in FACS at a concentration of 1 µg/million cell for 10 min at 4°C. After centrifugation and removal of excess Fc block, samples were stained with antibodies (listed below) for 20 min at 4°C in a staining volume of 300 µL. Samples were rinsed twice in ice-cold FACS and fixed in 500 µL 10% neutral buffered formalin (ThermoFisher Scientific, USA, Cat. No. 9990245) for 15 minutes at room temperature. Cells were scraped and transferred to a 96-well V-bottom plate for analysis by flow cytometry within 1 week.

In vitro and *in vivo* bioluminescence to CFU (BLI-CFU) correlation

A dilution series of *Pseudomonas aeruginosa* Xen 41 (PerkinElmer, MA, USA) was prepared in a black 96-well plate (ThermoFisher Scientific, USA, Cat. No. 165305) ranging from 10^0 to 10^7 CFU/well in a total volume of 100 µL. Samples were prepared in triplicate. CFU counts were verified by plating on nonselective LB agar plates. Bioluminescence imaging was performed on the Lago X *In Vivo* Imaging System (Spectral Instruments Imaging, USA). A series of exposures ranging from 5 s to 60 s were taken. The longest exposure without overexposure was used for analysis. The following imaging settings were used: F-stop 1.2, Binning: Heavy, FOV: 25. Images were analyzed using Aura version 4.0 (Spectral Instruments Imaging, USA) by integrating the radiance (photons/s/cm^2/sr) in a region of interest to measure total signal flux (photons/s). The linear regression and correlation were analyzed at bioluminescent flux ($\log_{10}$(photons/s) above 4 and 5 for *in vitro* and *in vivo,* respectively.

Delayed treatment mouse infection model

Male C57BL/6J mice were purchased from the Jackson Laboratory (Jackson Laboratory, #000664). All experiments and animal use procedures were approved by the Institutional Animal Care and Use Committee (IACUC) at the School of Medicine at Stanford University. The study design was adapted from previous work [101]. Briefly, 6-7-week-old male mice were anesthetized using 3% isoflurane and shaved. The shaved area was cleaned with povidone-iodine (Dynarex, USA, Cat. No. 1201) and isopropyl alcohol swabs. Mice received 0.1-0.5 mg/kg slow-release

buprenorphine (ZooPharm, USA) subcutaneously as an analgesic. A single circular midline dorsal full-thickness wound was created using a 6 mm biopsy punch (Integra Miltex, Catalog No.12-460-412). The wounds were immediately covered with Tegaderm (3M, USA, Cat. No. 1642W) with silicone adhesive (Vapon, USA, Cat. No. NTL1). Mice were placed in padded plastic collars (Saf-T-Shield, KVP International, USA, Cat. No. RCM) to prevent the removal of wound dressings. Mice received 500 µL of 0.9% normal saline by IP injection on the wounding day and food pellets covered with veterinary nutrient supplements (California Veterinary Supply, USA, Cat. No. HS-10033).

On the infection day, *Pa* Xen41 was grown in LB at 37°C with shaking to mid-log phase. Bacteria were pelleted by centrifugation, resuspended in PBS, diluted to 1.25 x 10^7 CFU/mL, and verified by plating on LB agar plates. 24 h post-wounding, wounds were inoculated with 40 µL Xen41 under Tegaderm using an insulin syringe (28G) at 5 x 10^5 CFU per wound. Bioluminescence images were obtained 1 h post-infection to confirm inoculum was properly injected under the Tegaderm.

24 h post-infection, all mice were imaged ("Day 1") before the first treatment. Mice were treated with 1) PBS as control; 2) dorsal penile vein injection (IV), 1 x 10^{11} PFU/mL; 3) high dose one-time topical bolus (HD), 1 x 10^{11} PFU/mL; 4) low dose one-time topical bolus (LD), 2.5 x 10^{10} PFU/mL; 5) daily topical bolus (DD), 2.5 x 10^{10} PFU/mL, for 4 days; or 6) HydroPhage (HP), 1 x 10^{11} PFU/mL. All mice were weighed daily. Additional Tegaderm dressings were applied on top of existing ones if the dressing became loose. Mice that removed Tegaderm dressings and had a resultant >2-log reduction in luminescent flux were excluded from subsequent analysis. Six days post-infection, mice were euthanized, and the wound was harvested (1 cm^2). Each wound was divided in half. Half of the wound was weighed and homogenized for enumerating colony-forming units (CFU) and plaque-forming units (PFU), and the other half was processed for flow cytometry. The next day, at least 10 colonies from each wound isolate were picked and started an overnight culture, then stored in 30% glycerol at -80°C for further characterization, such as quantification of phage resistance by PSA.

Bioluminescence imaging (BLI)

Bioluminescence imaging was performed on the Lago X *In Vivo* Imaging System (Spectral Instruments Imaging, USA). A series of exposures ranging from 5 s to 60 s were taken. The longest exposure without overexposure was used for analysis. The following imaging settings were used: F-stop 1.2, Binning: Heavy, FOV: 25. Images were analyzed using Aura version 4.0 (Spectral Instruments Imaging, USA) by integrating the radiance (photons/s/cm^2/sr) in a region of interest to measure total signal flux (photons/s).

Wound flow cytometry

Wounds were rinsed once in HBSS, blotted to remove excess HBSS, and placed into pre-weighed 1.5 mL polystyrene tubes containing 500 µL ice-cold digestion buffer (RPMI-1640 + 25 mM HEPES, pH 7.4, 1.3 WU/mL Liberase TL (Roche, Switzerland, Cat. No. 05401020001), 2 U/mL bovine DNase I (Roche, Switzerland, Cat. No. 11284932001), 25 mM $MgCl_2$, 1 mM $CaCl_2$, 200 U/mL collagenase IV (Worthington Biochemical, USA. Cat. No. LS004188). Samples were weighed and minced finely using scissors. An additional 500 µL ice-cold digestion buffer was added to samples and incubated at 37°C with shaking at 750 x rpm for 2 hours. Samples were inverted several times every 30 minutes during the incubation. After the 2-hour digestion, samples were treated with 100 µL Accutase (Innovative Cell Technologies, San Diego, CA, USA, Cat. No. AT104) and incubated for 20 minutes at room temperature.

Digested samples were passed through a 40 µm nylon cell strainer (Corning, Corning, NY, USA, Cat. No. 352340) pre-wetted with 1 mL of ice-cold FACS buffer (PBS + 1 mM EDTA + 1% BSA). Samples were pressed through the strainer using the rubber end of a syringe plunger. Cell strainers were rinsed with 5 mL of ice-cold FACS buffer. Cells were pelleted by centrifugation (500 x *g*, 10 min, 4°C), and the supernatant was aspirated. Pellets were resuspended in 1 mL ice-cold FACS buffer and pelleted again. Pellets were resuspended in 250 µL of room temperature ACK red blood cell lysis buffer (0.15 M NH_4Cl, 10 mM $KHCO_3$, 0.1 mM EDTA, pH 7.3) and incubated for precisely 4 minutes (variation <5 seconds), after which lysis was stopped by the addition of 750 µL of PBS.

Cells were then pelleted by centrifugation (500 x *g*, 20 min), removed supernatant, and resuspended in 200 µL ice-cold FACS buffer. 10 µL samples were diluted into a final volume of 200 µL and counted on a flow cytometer. 650,000 cells/sample were aliquoted to a 96-well V-bottom tissue culture-treated plate (Corning, Corning, USA, Cat. No. 07-200-96). The remaining cells were pooled and aliquoted for unstained, single-stained, and fluorescence-minus-one (FMO) controls.

For staining, cells were rinsed once in ice-cold FACS buffer and then stained in 50 µL 1:3000 IRDye 800CW Live/Dead NIR stain in PBS for 15 minutes at room temperature. Staining was quenched by the addition of 150 µL of ice-cold FACS buffer. After centrifugation, cells were resuspended in 30 µL of anti-mouse CD16/32 (Fc block) in FACS at a concentration of 1 µg/million cells for 10 min at 4°C. After centrifugation and removal of excess Fc block, samples were stained with antibodies (listed below) for 20 min at 4°C in a staining volume of 30 µL. Samples were then rinsed twice in ice-cold FACS and fixed in 200 uL 4% paraformaldehyde (20 min, room temperature). Samples were then resuspended in 200 µL FACS and acquired on the Cytek Aurora NL-3000 spectral flow cytometer (Cytek Biosciences, CA, USA) within 1 week of fixation. Spectral unmixing was performed using narrow gates and without unmixing autofluorescence.

Statistical analyses

Statistical analyses were performed using GraphPad Prism version 10. Ordinary one-way analysis of variance (ANOVA) with Tukey post-hoc tests was used for multiple comparisons unless otherwise noted. Unpaired two-tailed Student's *t*-tests were used for comparison between two groups unless otherwise mentioned. $P \leq 0.05$ was considered significant unless otherwise noted. Data were presented as mean with error bars representing the standard deviation (S.D.), unless otherwise noted. * $P \leq 0.05$, ** $P \leq 0.01$, *** $P \leq 0.001$, and **** $P \leq 0.0001$.

Acknowledgements

In vivo imaging was performed at Stanford Center for Innovation in *In Vivo* Imaging (Sci^3). We thank A. Khosravi, N. Nagy, A. Saraswathibhatla, and D. Indana and other members from Bollyky and Chaudhuri lab for their scientific inputs; the staff at the Sci^3 for providing the support needed to perform the required experiments, including F. Habte. The research reported in this publication was supported by a Stanford Catalyst Grant and a Stanford Coulter Translational Grant. Q. C. discloses support from Cystic Fibrosis Foundation CHEN21F0, Cystic Fibrosis Research Institute, and Stanford Maternal & Child Health Research Institute. T.D. discloses support from Stanford University Medical Scientist Training Program National Institutes of Health grant T32-GM007365; Stanford Interdisciplinary Graduate Fellowship affiliated with Sarafan ChEM-H, Gold Family Graduate Fellow. M.H. discloses support from National Institutes of Health grants R00-EB028838 and K99EB028838. O.C. acknowledges support from NIH grants R01 AR081993 and R01 GM148535. P.L.B discloses support from National Institutes of Health grant R01 HL148184-01; National Institutes of Health grant R01 AI12492093; National Institutes of Health grant R01 DC019965; Cystic Fibrosis Foundation grant; Emerson Collective grant. The contents are those of the authors and do not necessarily represent the views of the funding agencies.

Author contributions

Y.H.L., T.D., and Q.C. contributed equally. Y.H.L., T.D., Q.C., R.M., D.A., O.C., and P.L.B. conceived the study. Y.H.L. and R.M. performed hydrogel phage release pilot studies. Y.H.L., T.D., and Q.C. designed the experiments and mouse model. Y.H.L. and L.J.Z. performed rheological tests, and Y.H.L. conducted hydrogel degradation studies. Y.H.L., T.D., Q.C., L.J.Z., A.E., C.D.L., and W.S. performed *in vitro* phage release studies. Y.H.L., A.E., and Z.L. performed *in vitro* phage selection assays, and Y.H.L. conducted biofilm studies. T.D., N.A.P., and H.A.M. performed *in vitro* macrophage cytotoxicity and activation studies. Q.C., T.D., A.E., Y.H.L., L.J.Z., F.G.B., and T.H.W.C. performed *in vivo* studies, with C.D.L, Y.H.L., and A.E. curating data. M.H. conducted TEM imaging. A.E., A.H., and T.D. propagated and purified phages. Y.H.L., Q.C., T.D., and A.E. analyzed and interpreted the data. O.C. and P.L.B. supervised the study. Y.H.L., Q.C., T.D., O.C., and P.L.B. wrote the manuscript. All authors reviewed the manuscript.

Competing interests

The authors declare no competing interests

References

1. Sen, C. K. *et al.* Human skin wounds: a major and snowballing threat to public health and the economy. *Wound Repair Regen* **17**, 763–71 (2009).

2. Davies, D. Understanding biofilm resistance to antibacterial agents. *Nat Rev Drug Discov* **2**, 114–122 (2003).

3. Stevens, D. L. *et al.* Practice guidelines for the diagnosis and management of skin and soft tissue infections: 2014 update by the infectious diseases society of America. *Clinical Infectious Diseases* **59**, (2014).

4. Clinton, A. & Carter, T. Chronic wound biofilms: Pathogenesis and potential therapies. *Lab Medicine* **46**, 277–284 (2015).

5. Falanga, V. *et al.* Chronic wounds. *Nat Rev Dis Primers* **8**, 1–21 (2022).

6. Bowers, S. & Franco, E. Chronic wounds: Evaluation and management. *Am Fam Physician* **101**, 159–166 (2020).

7. Centers for Disease Control and Prevention. *National Diabetes Statistics Report Website*.

8. Kirketerp-Møller, K. *et al.* Distribution, organization, and ecology of bacteria in chronic wounds. *J Clin Microbiol* **46**, 2717–22 (2008).

9. Dowd, S. E. *et al.* Survey of bacterial diversity in chronic wounds using Pyrosequencing, DGGE, and full ribosome shotgun sequencing. *BMC Microbiol* **8**, 43 (2008).

10. Malic, S. *et al.* Detection and identification of specific bacteria in wound biofilms using peptide nucleic acid fluorescent in situ hybridization (PNA FISH). *Microbiology (N Y)* **155**, 2603–2611 (2009).

11. James, G. A. *et al.* Biofilms in chronic wounds. *Wound Repair and Regeneration* **16**, 37–44 (2008).

12. Lister, P. D., Wolter, D. J. & Hanson, N. D. Antibacterial-Resistant Pseudomonas aeruginosa : Clinical Impact and Complex Regulation of Chromosomally Encoded Resistance Mechanisms. *Clin Microbiol Rev* **22**, 582–610 (2009).

13. Kapel, N., Caballero, J. D. & MacLean, R. C. Localized pmrB hypermutation drives the evolution of colistin heteroresistance. *Cell Rep* **39**, 110929 (2022).

14. Olalekan, A. *et al.* High incidence of carbapenemase-producing *Pseudomonas aeruginosa* clinical isolates from Lagos, Nigeria. *JAC Antimicrob Resist* **5**, (2023).

15. Ogbolu, D. O., Piddock, L. J. V. & Webber, M. A. Opening Pandora's box: High-level resistance to antibiotics of last resort in Gram-negative bacteria from Nigeria. *J Glob Antimicrob Resist* **21**, 211–217 (2020).

16. Woodford, N., Palepou, M.-F. I., Babini, G., Bates, J. & Livermore, D. Carbapenemase-producing Pseudomonas aeruginosa in UK. *The Lancet* **352**, 546–547 (1998).

17. World Health Organization (WHO). *WHO Bacterial Priority Pathogens List*. *https://www.who.int/publications/i/item/9789240093461* (2024).

18. Centers for Disease Control and Prevention (CDC). Antibiotic Resistance Threats in The United States 2019. *https://www.cdc.gov/antimicrobial-resistance/data-research/threats/index.html* (2019).

19. Chen, Q. *et al.* Bacteriophage and Bacterial Susceptibility, Resistance, and Tolerance to Antibiotics. *Pharmaceutics* **14**, (2022).

20. d'Herelle, F. An Addresson BACTERIOPHAGY AND RECOVERY FROM INFECTIOUS DISEASES. *Can Med Assoc J* **24**, 619–28 (1931).

21. Wittebole, X., De Roock, S. & Opal, S. M. A historical overview of bacteriophage therapy as an alternative to antibiotics for the treatment of bacterial pathogens. *Virulence* **5**, 226–35 (2014).

22. Aslam, S. *et al.* Lessons learned from the first 10 consecutive cases of intravenous bacteriophage therapy to treat multidrug-resistant bacterial infections at a single center in the United States. *Open Forum Infect Dis* **7**, (2020).

23. Fiedler, A. W. *et al.* Phage therapy minimally affects the water microbiota in an Atlantic salmon (Salmo salar) rearing system while still preventing infection. *Sci Rep* **13**, 1–13 (2023).

24. Kovacs, C. J. *et al.* Disruption of Biofilm by Bacteriophages in Clinically Relevant Settings. *Mil Med* **00**, (2023).

25. Burrowes, B., Harper, D. R., Anderson, J., McConville, M. & Enright, M. C. Bacteriophage therapy: potential uses in the control of antibiotic-resistant pathogens. *Expert Rev Anti Infect Ther* **9**, 775–85 (2011).

26. Maddocks, S. *et al.* Bacteriophage Therapy of Ventilator-associated Pneumonia and Empyema Caused by Pseudomonas aeruginosa. *Am J Respir Crit Care Med* **200**, 1179–1181 (2019).

27. Cano, E. J. *et al.* Phage Therapy for Limb-threatening Prosthetic Knee Klebsiella pneumoniae Infection: Case Report and In Vitro Characterization of Anti-biofilm Activity. *Clin Infect Dis* **73**, e144–e151 (2021).

28. Chan, B. K. *et al.* Phage treatment of an aortic graft infected with *Pseudomonas aeruginosa*. *Evol Med Public Health* **2018**, 60–66 (2018).

29. Karinja, S. J. & Spector, J. A. Treatment of Infected Wounds in the Age of Antimicrobial Resistance: Contemporary Alternative Therapeutic Options. *Plast Reconstr Surg* **142**, 1082–1092 (2018).

30. Kutter, E. *et al.* Phage Therapy in Clinical Practice: Treatment of Human Infections. *Curr Pharm Biotechnol* **11**, 69–86 (2010).

31. Abedon, S. T., Kuhl, S. J., Blasdel, B. G. & Kutter, E. M. Phage treatment of human infections. *Bacteriophage* **1**, 66–85 (2011).

32. Międzybrodzki, R. *et al.* Pharmacokinetic and Pharmacodynamic Obstacles for Phage Therapy From the Perspective of Clinical Practice. *Clinical Infectious Diseases* **77**, S395–S400 (2023).

33. Dąbrowska, K. Phage therapy: What factors shape phage pharmacokinetics and bioavailability? Systematic and critical review. *Med Res Rev* **39**, 2000–2025 (2019).

34. Yip, Y. L., Hawkins, N. J., Smith, G. & Ward, R. L. Biodistribution of filamentous phage-Fab in nude mice. *J Immunol Methods* **225**, 171–178 (1999).

35. Lin, Y. W. *et al.* Pharmacokinetics/pharmacodynamics of antipseudomonal bacteriophage therapy in rats: a proof-of-concept study. *Clinical Microbiology and Infection* **26**, 1229–1235 (2020).

36. Tiwari, B. R., Kim, S., Rahman, M. & Kim, J. Antibacterial efficacy of lytic Pseudomonas bacteriophage in normal and neutropenic mice models. *The Journal of Microbiology* **49**, 994–999 (2011).

37. PAYNE, R. J. H. & JANSEN, V. A. A. Understanding Bacteriophage Therapy as a Density-dependent Kinetic Process. *J Theor Biol* **208**, 37–48 (2001).

38. Dąbrowska, K. & Abedon, S. T. Pharmacologically Aware Phage Therapy: Pharmacodynamic and Pharmacokinetic Obstacles to Phage Antibacterial Action in Animal and Human Bodies. *Microbiology and Molecular Biology Reviews* **83**, (2019).

39. El Haddad, L., Harb, C. P., Gebara, M. A., Stibich, M. A. & Chemaly, R. F. A Systematic and Critical Review of Bacteriophage Therapy Against Multidrug-resistant ESKAPE Organisms in Humans. *Clinical Infectious Diseases* **69**, 167–178 (2019).

40. Duplessis, C. A. & Biswas, B. A Review of Topical Phage Therapy for Chronically Infected Wounds and Preparations for a Randomized Adaptive Clinical Trial Evaluating Topical Phage Therapy in Chronically Infected Diabetic Foot Ulcers. *Antibiotics (Basel)* **9**, (2020).

41. Mendes, J. J. *et al.* Wound healing potential of topical bacteriophage therapy on diabetic cutaneous wounds. *Wound Repair and Regeneration* **21**, 595–603 (2013).

42. Chhibber, S., Kaur, J. & Kaur, S. Liposome Entrapment of Bacteriophages Improves Wound Healing in a Diabetic Mouse MRSA Infection. *Front Microbiol* **9**, (2018).

43. Steele, A., Stacey, H. J., de Soir, S. & Jones, J. D. The Safety and Efficacy of Phage Therapy for Superficial Bacterial Infections: A Systematic Review. *Antibiotics (Basel)* **9**, (2020).

44. Zyman, A., Górski, A. & Międzybrodzki, R. Phage therapy of wound-associated infections. *Folia Microbiol (Praha)* **67**, 193–201 (2022).

45. Kim, H. Y., Chang, R. Y. K., Morales, S. & Chan, H. K. Bacteriophage-delivering hydrogels: Current progress in combating antibiotic resistant bacterial infection. *Antibiotics* **10**, 1–17 (2021).

46. Chang, R. Y. K., Morales, S., Okamoto, Y. & Chan, H.-K. Topical application of bacteriophages for treatment of wound infections. *Transl Res* **220**, 153–166 (2020).

47. Vonasek, E., Lu, P., Hsieh, Y.-L. & Nitin, N. Bacteriophages immobilized on electrospun cellulose microfibers by non-specific adsorption, protein–ligand binding, and electrostatic interactions. *Cellulose* **24**, 4581–4589 (2017).

48. Morozova, V. V, Kozlova, Y. N., Ganichev, D. A. & Tikunova, N. V. Bacteriophage Treatment of Infected Diabetic Foot Ulcers. *Methods Mol Biol* **1693**, 151–158 (2018).

49. Nube, V. L., Alison, J. A. & Twigg, S. M. Frequency of sharp wound debridement in the management of diabetes-related foot ulcers: exploring current practice. *J Foot Ankle Res* **14**, 1–7 (2021).

50. Shafigh Kheljan, F. *et al.* Design of Phage-Cocktail–Containing Hydrogel for the Treatment of Pseudomonas aeruginosa–Infected Wounds. *Viruses* **15**, 803 (2023).

51. Patpatia, S. *et al.* Rapid hydrogel-based phage susceptibility test for pathogenic bacteria. *Front Cell Infect Microbiol* **12**, 1032052 (2022).

52. Kalelkar, P. P., Riddick, M. & García, A. J. Biomaterial-based antimicrobial therapies for the treatment of bacterial infections. *Nat Rev Mater* **7**, 39–54 (2022).

53. Bai, H. *et al.* Phage-Based antibacterial hydrogels for bacterial targeting and Ablation: Progress and perspective. *European Journal of Pharmaceutics and Biopharmaceutics* **198**, 114258 (2024).

54. Ma, Y. *et al.* Microencapsulation of bacteriophage felix O1 into chitosan-alginate microspheres for oral delivery. *Appl Environ Microbiol* **74**, 4799–805 (2008).

55. Korehei, R. & Kadla, J. F. Encapsulation of T4 bacteriophage in electrospun poly(ethylene oxide)/cellulose diacetate fibers. *Carbohydr Polym* **100**, 150–7 (2014).

56. Barros, J. A. R. *et al.* Encapsulated bacteriophages in alginate-nanohydroxyapatite hydrogel as a novel delivery system to prevent orthopedic implant-associated infections. *Nanomedicine* **24**, (2020).

57. Rubalskii, E. *et al.* Fibrin glue as a local drug-delivery system for bacteriophage PA5. *Sci Rep* **9**, 3–10 (2019).

58. Wroe, J. A., Johnson, C. T. & García, A. J. Bacteriophage delivering hydrogels reduce biofilm formation in vitro and infection in vivo. *J Biomed Mater Res A* **108**, 39–49 (2020).

59. Markoishvili, K. *et al.* A novel sustained-release matrix based on biodegradable poly(ester amide)s and impregnated with bacteriophages and an antibiotic shows promise in management of infected venous stasis ulcers and other poorly healing wounds. *Int J Dermatol* **41**, 453–458 (2002).

60. Wang, R., Yeh, Y. J., An, Y. N. & Virly. Engineering pH-sensitive erodible chitosan hydrogel composite containing bacteriophage: An interplay between hydrogel and bacteriophage against Staphylococcus aureus. *Int J Biol Macromol* **253**, 127371 (2023).

61. Tsai, C.-C. *et al.* Injectable, Shear-Thinning, Self-Healing, and Self-Cross-Linkable Benzaldehyde-Conjugated Chitosan Hydrogels as a Tissue Adhesive. *Biomacromolecules* **25**, 1084–1095 (2024).

62. Basu, S., Pacelli, S. & Paul, A. Self-healing DNA-based injectable hydrogels with reversible covalent linkages for controlled drug delivery. *Acta Biomater* **105**, 159–169 (2020).

63. McKinnon, D. D., Domaille, D. W., Cha, J. N. & Anseth, K. S. Biophysically defined and cytocompatible covalently adaptable networks as viscoelastic 3d cell culture systems. *Advanced Materials* **26**, 865–872 (2014).

64. Kölmel, D. K. & Kool, E. T. Oximes and Hydrazones in Bioconjugation: Mechanism and Catalysis. *Chem Rev* **117**, 10358–10376 (2017).

65. Burgener, E. B. & Bollyky, P. L. The Rational Design of Broadly Effective Phage Therapy Cocktails Against Bacterial Infections.

66. Malone, M. *et al.* The prevalence of biofilms in chronic wounds: a systematic review and meta-analysis of published data. *J Wound Care* **26**, 1–5 (2017).

67. Costerton, J. W., Stewart, P. S. & Greenberg, E. P. Bacterial biofilms: a common cause of persistent infections. *Science (1979)* **284**, 1318–1322 (1999).

68. Vlamakis, H., Chai, Y., Beauregard, P., Losick, R. & Kolter, R. Sticking together: building a biofilm the Bacillus subtilis way. *Nat Rev Microbiol* **11**, 157–168 (2013).

69. Mann, E. E. & Wozniak, D. J. Pseudomonas biofilm matrix composition and niche biology. *FEMS Microbiol Rev* **36**, 893–916 (2012).

70. Parsek, M. R. & Singh, P. K. Bacterial biofilms: an emerging link to disease pathogenesis. *Annu Rev Microbiol* **57**, 677–701 (2003).

71. Uberoi, A., McCready-Vangi, A. & Grice, E. A. The wound microbiota: microbial mechanisms of impaired wound healing and infection. *Nat Rev Microbiol* (2024) doi:10.1038/s41579-024-01035-z.

72. Chegini, Z. *et al.* Bacteriophage therapy against Pseudomonas aeruginosa biofilms: A review. *Ann Clin Microbiol Antimicrob* **19**, 1–17 (2020).

73. Haines, M. E. K. *et al.* Analysis of Selection Methods to Develop Novel Phage Therapy Cocktails Against Antimicrobial Resistant Clinical Isolates of Bacteria. *Front Microbiol* **12**, 1–15 (2021).

74. Bach, M. S. *et al.* Filamentous bacteriophage delays healing of Pseudomonas-infected wounds. *Cell Rep Med* **3**, 100656 (2022).

75. de Vries, C. R. *et al.* A delayed inoculation model of chronic pseudomonas aeruginosa wound infection. *Journal of Visualized Experiments* **2020**, 1–6 (2020).

76. Sweere, J. M. *et al.* The Immune Response to Chronic Pseudomonas aeruginosa Wound Infection in Immunocompetent Mice. *Adv Wound Care (New Rochelle)* **9**, 35–47 (2020).

77. Kaur, P., Gondil, V. S. & Chhibber, S. A novel wound dressing consisting of PVA-SA hybrid hydrogel membrane for topical delivery of bacteriophages and antibiotics. *Int J Pharm* **572**, 118779 (2019).

78. Shen, H. Y. *et al.* Controlled-release of free bacteriophage nanoparticles from 3D-plotted hydrogel fibrous structure as potential antibacterial wound dressing. *Journal of Controlled Release* **331**, 154–163 (2021).

79. Chang, R. Y. K., Okamoto, Y., Morales, S., Kutter, E. & Chan, H. K. Hydrogel formulations containing non-ionic polymers for topical delivery of bacteriophages. *Int J Pharm* **605**, 120850 (2021).

80. Agarwal, R. *et al.* Inhaled bacteriophage-loaded polymeric microparticles ameliorate acute lung infections. *Nat Biomed Eng* **2**, 841–849 (2018).

81. Bean, J. E. *et al.* Triggered release of Bacteriophage K from agarose/hyaluronan hydrogel matrixes by staphylococcus aureus virulence factors. *Chemistry of Materials* **26**, 7201–7208 (2014).

82. Ren, H. *et al.* Injectable, self-healing hydrogel adhesives with firm tissue adhesion and on-demand biodegradation for sutureless wound closure. *Sci Adv* **9**, eadh4327 (2023).

83. Roth, J. G. *et al.* Tunable hydrogel viscoelasticity modulates human neural maturation. *Sci Adv* **9**, eadh8313 (2023).

84. Sharma, P. K. & Singh, Y. Glyoxylic Hydrazone Linkage-Based PEG Hydrogels for Covalent Entrapment and Controlled Delivery of Doxorubicin. *Biomacromolecules* **20**, 2174–2184 (2019).

85. Hua, Y. *et al.* Adaptable to Mechanically Stable Hydrogels Based on the Dynamic Covalent Cross-Linking of Thiol-Aldehyde Addition. *ACS Macro Lett* **8**, 310–314 (2019).

86. Berkson, J. D. *et al.* Phage-specific immunity impairs efficacy of bacteriophage targeting Vancomycin Resistant Enterococcus in a murine model. *Nat Commun* **15**, 1–14 (2024).

87. Biswas, B. *et al.* Bacteriophage Therapy Rescues Mice Bacteremic from a Clinical Isolate of Vancomycin-Resistant Enterococcus faecium. *Infect Immun* **70**, 1664 (2002).

88. Echterhof, A. *et al.* The contribution of neutrophils to bacteriophage clearance and pharmacokinetics in vivo. *bioRxiv* (2024) doi:10.1101/2024.01.25.577154.

89. Pirnay, J. P. *et al.* Personalized bacteriophage therapy outcomes for 100 consecutive cases: a multicentre, multinational, retrospective observational study. *Nat Microbiol* **9**, (2024).

90. Chadha, P., Katare, O. P. & Chhibber, S. In vivo efficacy of single phage versus phage cocktail in resolving burn wound infection in BALB/c mice. *Microb Pathog* **99**, 68–77 (2016).

91. Horowitz, A., Stegmann, K. A. & Riley, E. M. Activation of natural killer cells during microbial infections. *Front Immunol* **2**, 1–13 (2012).

92. Esin, S. *et al.* Direct binding of human NK cell natural cytotoxicity receptor NKp44 to the surfaces of mycobacteria and other bacteria. *Infect Immun* **76**, 1719–1727 (2008).

93. Mody, C. H. *et al.* Microbial killing by NK cells. *J Leukoc Biol* **105**, 1285–1296 (2019).

94. Sobecki, M. *et al.* NK cells in hypoxic skin mediate a trade-off between wound healing and antibacterial defence. *Nat Commun* **12**, 4700 (2021).

95. Liu, D. *et al.* The safety and toxicity of phage therapy: A review of animal and clinical studies. *Viruses* **13**, 1–20 (2021).

96. Chung, K. M., Nang, S. C. & Tang, S. S. The Safety of Bacteriophages in Treatment of Diseases Caused by Multidrug-Resistant Bacteria. *Pharmaceuticals* **16**, (2023).

97. Kavitha, K. V. Choice of wound care in diabetic foot ulcer: A practical approach. *World J Diabetes* **5**, 546 (2014).

98. Dhivya, S., Padma, V. V. & Santhini, E. Wound dressings - A review. *BioMedicine (Netherlands)* **5**, 24–28 (2015).

99. Sood, A., Granick, M. S. & Tomaselli, N. L. Wound Dressings and Comparative Effectiveness Data. *Adv Wound Care (New Rochelle)* **3**, 511–529 (2014).

100. Dharmaraj, T. *et al.* Rapid assessment of changes in phage bioactivity using dynamic light scattering. *PNAS Nexus* **2**, (2023).

101. Chen, J. S., Longaker, M. T. & Gurtner, G. C. Murine models of human wound healing. *Methods Mol Biol* **1037**, 265–74 (2013).